PalZ
https://doi.org/10.1007/s12542-025-00739-8

RESEARCH PAPER

Early Pleistocene rhinoceroses (Mammalia, Perissodactyla, Rhinocerotidae) from Northern Greece: biochronological and paleobiogeographic implications

Krystalia Chitoglou[1,3] · Luca Pandolfi[2] · George E. Konidaris[1,3] · Dimitris S. Kostopoulos[3]

Received: 10 September 2024 / Accepted: 6 June 2025

Abstract
Rhinoceroses were well-distributed across Southern Europe during the Early Pleistocene with abundant remains, but they are rather scarce in the Greek record and even less studied from a systematic point of view. In this article, we study a total of 124 specimens from eight fossil-bearing Lower Pleistocene localities of Northern Greece, spanning from ~ 2.3 to ~ 1.2 Ma. The localities of Tsiotra Vryssi and Krimni in the Mygdonia Basin provided the best material in terms of both number and preservation of specimens, whereas in the rest of the sites from Mygdonia, Drama and Neapolis-Grevena Basins less than ten specimens for each site are known. The present study documents the first occurrence in Greece of *Stephanorhinus* cf. *S. hundsheimensis* in the localities of Riza-1, Krimni-1, 3 and Tsiotra Vryssi, which suggests that the species may have entered earlier than the rest of the Europe. Additionally, the last occurrence of *Stephanorhinus jeanvireti* in Greece is recorded in Dafnero-3. The presence of *Stephanorhinus etruscus* is confirmed in several localities including Volax, Tsiotra Vryssi, Libakos and Apollonia-1, and indicates a chronological range from ~ 2.3 to ~ 1.2 Ma. At the beginning of this time frame both *S. jeanvireti* and *S. etruscus* co-occur in Greece, whereas the presence of both *S. etruscus* and *Stephanorhinus* cf. *S. hundsheimensis* at Tsiotra Vryssi testifies their first local co-occurrence.

Keywords *Stephanorhinus* · Morphology · Biostratigraphy · Mygdonia · Villafranchian

Introduction

Whilst they are no longer existing in Greece, rhinoceroses were once a common faunal element in the fossil assemblages of the wider region. Representatives of the family Rhinocerotidae were abundant in Greece during the Late Miocene, became rare during the Pliocene, and they were usually scarce during the Pleistocene (Giaourtsakis, 2022). The significant faunal turnover at the end of the Miocene, associated with the Messinian Salinity Crisis, resulted in the extinction of several rhinocerotid lineages that previously thrived in the Pikermian biochrono-faunas (Giaourtsakis, 2022). During the Pliocene, new genera such as *Pliorhinus* Pandolfi, Pierre-Olivier, Bukhsianidze, Lordkipanidze, Rook, 2021 and *Stephanorhinus* Kretzoi, 1942, occurred in Europe and Greece (Tsoukala, 2018; Chitoglou et al., 2023). *Stephanorhinus* became soon the dominant rhinocerotid genus of the Pleistocene in the whole Eurasia, with several species succeeding in time, while *Coelodonta* Bronn, 1831 first occurred in Asia during the mid Pliocene and spread in Europe during the Middle Pleistocene (Puzachenko et al., 2021). The occurrences of these taxa in Greece are scantly and poorly documented, leaving a gap in our knowledge on their dispersal pattern, biochronology and evolution.

Over the past few decades, systematic excavations in several old and new Pleistocene localities of Greece unearthed a significant number of rhinoceros remains. Despite that their record is not as extensive as in other European countries,

Handling editor: Thomas Mörs.

✉ Krystalia Chitoglou
krystalia.chitoglou@uni-tuebingen.de

[1] Paleoanthropology, Institute for Archaeological Sciences and Senckenberg Centre for Human Evolution and Palaeoenvironment, Department of Geosciences, Eberhard Karls University of Tübingen, Tübingen, Germany

[2] Dipartimento di Scienze della Terra, Università di Pisa, Via S. Maria 53, 56126 Pisa, Italy

[3] Laboratory of Geology and Palaeontology, School of Geology, Aristotle University of Thessaloniki, Thessaloníki, Greece

Published online: 29 September 2025

it is nonetheless sufficient (a) to provide valuable insights regarding the expansion of several rhinoceros' lineages in the southern Balkans and (b) to offer important data on their chronostratigraphic ranges. The aim of the herein study is to provide a taxonomic revision of the older material and to present newly discovered specimens from several Lower Pleistocene localities of Greece in order to enhance our understanding of the chronology/biostratigraphy and biogeography, as well as niche partitioning, of *Stephanorhinus* species at the eastern corner of peri-Mediterranean Europe, improving our knowledge at a European scale.

Materials and methods

The material of this study (124 specimens) originates from the Lower Pleistocene localities of Dafnero-3 (DFN3) and Libakos (LIB) in the Grevena-Neapolis Basin, Volax (VOL) in the Drama Basin, and several sites in Mygdonia Basin (Fig. 1). All specimens are stored at the Museum of Geology-Paleontology-Paleoanthropology of the Laboratory of Geology and Palaeontology, University of Thessaloniki, Greece (LGPUT). DFN-3 and VOL yielded a MNQ17 large mammal assemblage and are dated at ca. 2.5–2.3 Ma (e.g., Kostopoulos et al., 2019; Benammi et al., 2020; Konidaris & Kostopoulos, 2024). The geological, stratigraphic, and chronological background of those sites are given in Kostopoulos (1996), Koufos and Vlachou (1997), Koufos (2001), and Benammi et al. (2020). The stratigraphic and geological context of LIB is provided by Steensma (1988), and Koufos and Tamvakis (2022). The site provided a large mammal assemblage biochronologically dated to ca. 1.6–1.5 Ma (Konidaris & Kostopoulos, 2024).

The material from Mygdonia Basin comes from Tsiotra Vryssi (TSR), Krimni-1 (KRI), Krimni-3 (KMN), Platanochori-1 (PLN), Apollonia-1 (APL), and Riza-1 (RIZ) (Fig. 1). The geology and stratigraphy of the basin has been already described in detail by Koufos et al. (1995) and Konidaris et al. (2015). TSR, KRI and KMN are placed in the upper parts of the Gerakarou Formation (Fm) and yielded vertebrate assemblages dated between 1.78 and ~ 1.5 (Konidaris et al., 2015, 2021, 2022; Kostopoulos et al., 2023; Konidaris & Kostopoulos, 2024). PLN, APL, and RIZ belong to the overlain Platanochori Fm, and are biochronologically dated to ca. 1.2 Ma (Konidaris et al., 2015; Konidaris & Kostopoulos, 2024).

The dental nomenclature is based on Guérin (1980) and Lacombat (2006). The upper-case letters P and M denote the upper premolars and molars, respectively, and the lower-case p and m the corresponding lower ones. Cranial and postcranial terminology follows Guèrin (1980) and Mazza (1988); particularly for the vertebra we use Tong and Wang (2014) and for the limb bones, we use a combination of terminology proposed by Mazza (1988) and Mallet et al. (2019).

Measurements were taken with a digital caliper at 0.01 mm precision. All data were analyzed with the software R (Core Team, 2020). The revised Quaternary time scale (Gibbard et al., 2010) is used for chronological references in this text; the Miocene/Pliocene and the Pliocene/Pleistocene boundaries are placed at 5.4 Ma and 2.6 Ma, respectively.

Measurements for biometrical comparisons are based on the original study of material from Kalamoto-1 and Kalamoto-2 (Palaeontological Exhibition of Kalamoto, Greece), Upper Valdarno, Pirro Nord and Olivola (Geological and Paleontological Section of the Natural History Museum of Florence, Italy, IGF-NHMF), and from available literature (Guérin & Heintz, 1971; Guérin, 1972, 1973; Caloi & Palombo, 1978; Mazza, 1988; Fortelius et al., 1993; Mazza et al., 1993; Kahlke, 2001; Guérin, 2004; Lacombat, 2005; Lacombat & Moullé, 2005; Pandolfi & Petronio, 2011; Guérin & Tsoukala, 2013; Pandolfi, 2013; Pandolfi & Tagliacozzo, 2015; Tsoukala & Guérin, 2016; Pandolfi et al., 2017; Tsoukala, 2018; García-Fernández et al., 2023; Stefanelli et al., 2024). Measurements abbre of the materials studied are given in the Appendix (SI Table 1). Raw data of comparative material is available on request.

The systematics of Rhinocerotidae is still troublesome and the revision of previously studied material results in its assignment into different species. Due to this fact, the morphological conclusions provided by Guérin (1980) are referred here only for historical reasons. For the same reason, the size-range given by the same author for several postcranial bones are precluded.

Institutional abbreviations. Museum of Geology-Paleontology-Paleoanthropology of the Laboratory of Geology and Palaeontology, Aristotle University of Thessaloniki, Greece (LGPUT); IGF-NHMF, Geological and Paleontological Section of the Natural History Museum of Florence, Italy; NMB, Naturhistorisches Museum, Basel, Switzerland.

Scientific abbreviations. APDS (in long bones): antero-posterior diameter of the shaft; C3 for the third vertebra; DAPD: distal antero-posterior diameter; DP for deciduous teeth; DTD: distal transversal diameter; Fm: Formation; Hm: medial height; Hmax: maximal height; Lmax: maximal length; M/m: for molars; Mc: Metacarpals; McIII: third metacarpal; McIV: fourth metacarpal; Mt: metatarsal; MtII: second metatarsal; MtIII: third metatarsal; MtIV: fourth metatarsal; P/p for premolars; PAPD: proximal antero-posterior diameter; PTD: proximal transversal diameter; TDS: transversal diameter of the shaft.

Systematic Paleontology

Order **Perissodactyla** Owen, 1848

Family **Rhinocerotidae** Gray, 1821

Tribe **Rhinocerotini** Gray, 1821

Genus ***Stephanorhinus*** Kretzoi, 1942

Type species. *Stephanorhinus etruscus* (Falconer, 1868)

Remarks: The studied specimens fit within the synapomorphic features (cfr. Pandolfi, 2023) described for the genus: the teeth are partially hypsodont, the antecrochet is usually absent, the distal articulation of the humerus is diabolo-shaped, the posterior border of the astragal trochlea, in proximal view, is sinuous, and the insertion of the muscle *fibularis longus* on the calcaneus is not visible. Furthermore, the postcranial remains are generally slender and longer than *Coelodonta*, and less massive than *Rhinoceros*. Contrary to *Dicerorhinus*, metapodials display low and smooth intermediate reliefs, the proximal border of the *patellar trochlear* is curved and the cuboid-facet on MtIII is absent. Contrary to *Dicerorhinus* and *Rhinoceros*, the articular facet for the fibula is absent on the calcaneus, tibia and fibula are in contact or fused and the *fovea capitis* is high and narrow. Contrary to *Rhinoceros,* the trochlear notch is absent on the astragalus, the trochanter major is high, the insertion of the *extensor carpalis* on the metacarpals is flat, and the posterior apophysis of the tibia is generally high. Differences between *Stephanorhinus* and *Pliorhinus* are listed in Pandolfi et al. (2021a), while additional differences between *Stephanorhinus* and *Coelodonta* can be deduced from Uzunidis et al. (2022). Considering the general morphology of the studied remains and the considerations reported above, we can confidently assign all the studied remains to *Stephanorhinus*.

Stephanorhinus cf. ***S. jeanvireti*** (Guérin, 1972)

Material. McIII, DFN3-340

Description and comparison. **McIII.** DFN3-340 is completely preserved, but it is antero-posteriorly compressed (Fig. 2b–d). In proximal view, the anterior border of the proximal epiphysis is convex; the proximal articular surface has a rather pentagonal shape. In anterior view, the proximal border is concave and protrudes proximally. In lateral view, the posterior-proximal articular surface is flat, almost triangular, but elongated proximo-distally. In medial view, the medial-proximal articular surface is flat, oval-shaped and in contact with the proximal articular surface, creating a crest. The diaphysis is transversally developed, although it is crashed. In anterior view, the distal articular surface is symmetrical with a convex proximal border. The articular

Fig. 1 Studied fossiliferous localities: Dafnero-3 (DFN3), Volax (VOL), Tsiotra Vryssi (TSR), Libakos (LIB), Krimni-1 (KRI), Krimni-3 (KMN), Platanochori-1 (PLN), Riza-1 (RIZ), Apollonia-1 (APL), satellite image from Google Earth

surface is narrower than the distal epiphysis and the lateral trochlea slightly greater extended than the medial one.

Remarks. DFN3-340 differs from *S. etruscus* in the wider proximal articular surface, and the concave anterior border in proximal view. It differs from *S. hundsheimensis* in the more protruding medial crest and the more concave proximal border in anterior view. Unlike DFN3-340, in the McIII of *S. hemitoechus* a groove delimits the proximal articular surface in anterior view, whereas the distal articular surface has the same width as the distal epiphysis (Pandolfi & Tagliacozzo, 2015). In proximal view, DFN3-340 differs from *S. kirchbergensis,* in the more elongated transversally than antero-posteriorly proximal articular surface (Kahlke, 1975). DFN3-340 shares common characters with *S. jeanvireti*, such as the concave proximal border in anterior view and the protruding crest (Tsoukala, 2018). However, it differs from *S. jeanvireti* from Millia, in the more transversally elongated proximal articular surface (Guérin & Tsoukala, 2013).

Stephanorhinus etruscus (Falconer, 1868).

Material. Distal epiphysis of humeri, TSR-133, LIB-497, APL-408; proximal epiphysis of ulnae, TSR-G21-73, APL-348; proximal epiphysis of radii, TSR-C17-7, TSR-G21-72, APL-278; proximal epiphysis of McIII, TSR-36; distal epiphysis of tibiae, TSR-50, VOL-215; astragalus, APL-213; calcanei, APL-213b, LIB-180; navicular, TSR-F18-64b; cuboid, TSR-F18-64b; first cuneiform, TSR-F18-64b; second cuneiform, TSR-F18-64b; third cuneiform, TSR-F18-64b; MtIIs, TSR-F18-64a, APL-931, APL-845; MtIII, TSR-F18-64a; MtIV, TSR-F18-64a.

Descriptions and comparisons. **Humerus.** The humeri LIB-497(SI Fig. S1), TSR-133 (Fig. 3, a) and APL-408 (Fig. 3b) preserve a convex medial border of the medial lip of the distal trochlea. The distal trochlea of LIB-497 and APL-408 is asymmetric and slightly tilted; the groove separating the medial and lateral lips is wide and deep. In LIB-497 the lateral epicondyle is twice the size of the medial one whereas in APL-408 is damaged. In posterior view, the olecranon fossa of TSR-133 and APL-408 is wide and triangularly shaped. Additionally, the epicondylar crest is very well marked in APL-408, and the coronoid fossa is wide, deep, and relatively high.

Remarks. The dimensions of the humerus diaphyses LIB-497 and TSR-133 fall into the range of the larger-sized humeri of *S. etruscus* and the smaller-sized specimens of *S. hundsheimensis.* APL-408 falls into the range of *S. hundsheimensis,* and close to *S. etruscus* (Fig. 4).

In anterior view, LIB-497 differs from APL-408, TSR-G19-13 and TSR-L21-19 at the shallow and curved anterior border of the trochlea groove which are characters similar to *S. etruscus* from Poggio Rosso (Italy, IGF-NHMF). In distal view, although they are all very similar, LIB-497 has a stronger lateral condyle. The trochlea of TSR-133 and APL-408 is oblique, and the medial border of its medial lip is straight and oblique, characters similar to *S. etruscus* from Poggio Rosso. APL-408 has wide and profound olecranon fossa with triangular outline as is reported for *S. etruscus* (Fortelius et al., 1993) and different from *S. hundsheimensis* (García-Fernández et al., 2023). All the studied specimens differ from *S. hemitoechus* since the latter preserves a sinuous medial border of the medial lip of the trochlea and a shallower trochlea groove (Pandolfi & Tagliacozzo, 2015).

Radius and ulna. TSR-G21-73 is a quite well-preserved ulna (not preserving the olecranon) that articulates with the radius TSR-G21-72. Both TSR-G21-73 and APL-348 (SI Fig. S2), preserve an asymmetrical trochlear notch, with a small difference in height between the distal edges of the medial and lateral articular surfaces. The lateral articular surface is wider than the medial one and parallel to the corpus of the bone. In lateral view, there is a moderately marked groove laterally to the trochlear notch, and the anconeal process projects strongly anteriorly. Additionally, in APL-348 there is a strong depression distally the trochlear notch and the preserved lateral articular surface for the radius resembles a stripe that is narrower at the lateral part.

The radii TSR-G21-72, TSR-C17-7 (Fig. 3c, d) and APL-278 (SI Fig. S2) preserve only the proximal epiphysis and part of the diaphysis. In proximal view, the medial articular surface is subelliptical with convex anterior border and the lateral one is subsquared (damaged in APL-278). The posterior border of the articulation of TSR-G21-72 and TSR-C17-7 forms a 120^{o} angle. In anterior view, the coronoid process is prominent (TSR-G21-72) or slightly prominent (TSR-C17-7); it is damaged in APL-278 and the *brachii biceps* are hardly distinguishable. In posterior view, the shape of the medial articular surface is like a reduced elongated stripe (TSR-G21-72 and TSR-C17-7) while the lateral one is triangular and in TSR-C17-7 moderately high.

Remarks. The specimens TSR-G21-73 and APL-348 are assigned to *S. etruscus* because they were found articulated with the radii TSR-G21-72 and APL-278 respectively. The proximal articular surface for the radius is proposed as diagnostic between *S. hundsheimensis* and *S. hemitoechus* (Lacombat, 2005), and the ulna of *S. kirchbergensis* is generally larger than those of other *Stephanorhinus* species, but a morphometric discrimination between *S. etruscus* and *S. hundsheimensis* seems difficult based on currently known data (e.g., Fortelius et al., 1993).

The radii APL-278, TSR-C17-7 and TSR-G21-72 share common characters with *S. etruscus,* such as the weakly

Fig. 2 Rhinoceros specimens from Dafnero-3 (DFN3). **a** Premolar (DFN3-341) of *Stephanorhinus* sp. in occlusal view; **b–d** left McIII of *Stephanorhinus* cf. *S. jeanvireti* (DFN3-340) in **b** proximal, **c** anterior and **d**, posterior views. Scale bar equals 5 cm

concave and oblique posterior lateral border in proximal view, the moderate concavity of the anterior border at the level of the coronoid process, and the ~ 120° angle between the posterior borders of the proximal articulation (Fortelius et al., 1993). These characters additionally distinguish them from S. *hundsheimensis* (Kahlke, 2001). In anterior view, the proximal border of TSR-C17-7 is undulated forming a more obtuse angle, with a less protruding coronoid process than the TSR-G21-72. They both differ from *S. jeanvireti* in the more concave anterior border in proximal view (Tsoukala, 2018). The specimen APL-278 differs from *S. hemitoechus*, as in proximal view the latter species has much stronger concavity at the anterior border and it is more concave at the postero-lateral border (Pandolfi & Tagliacozzo, 2015). The specimens from TSR and APL have sub-elliptical medial and sub-square lateral articular surfaces, which are different from the sub-circular and sub-square shaped surfaces, respectively of *S. hemitoechus* (Pandolfi & Tagliacozzo, 2015).

McIII. In proximal view, the anterior border of TSR-36 (Fig. 3e, f) is slightly convex; the proximal articular surface is trapezoidal, convex antero-posteriorly, and concave proximo-laterally. In anterior view, the crest separating the proximal articular surface from the lateral one for the uncinate is sharp. In lateral view, the proximo-posterior articular surface protrudes posteriorly, and it is flat, large, and oval-shaped. The two articular surfaces of the proximo-lateral side are separated by a deep, and wide groove. In medial view, the articular surface for the McII is semi-circular and flat.

Remarks. TSR-36 is similar to *S. etruscus* from Poggio Rosso in the morphology of the proximal articular surface in anterior view. It differs thought in the more compressed diaphysis. In anterior view, the preserved proximal articular surface of TSR-36, differs from the McIII of *S. hundsheimensis* in the slightly more acute angle between the lateral articular surface for the uncinate and that for the McIV (García-Fernández et al., 2023; Stefanelli et al., 2024). A sub-trapezoidal or trapezoidal proximal articular surface of McIII is reported as diagnostic of *S. hundsheimensis* as opposed to the sub triangular surface of *S. etruscus* (Lacombat, 2005; Pandolfi et al., 2018; Stefanelli et al., 2024), but the McIII of *S. hundsheimensis* from Cova del Rinoceront (individual #8096, from La Guixera laboratory (Castelldefels City Council)), have a triangular outline (García-Fernández et al., 2023). TSR-36 preserves a trapezoidal outline of the proximal articular surface for the magnum, but the character seems in our opinion insufficient to discriminate between *S. etruscus* and *S. hundsheimensis*. TSR-36 differs from *S. kirchbergensis* in the concave anterior border in proximal view (Kahlke, 1975), the much higher medial part of the articulation in anterior view, and the more distally located medial tuberosity in anterior view (Lobachev et al., 2021). Similarly, TSR-36 differs from *S. hemitoechus*, in which the proximal articular surface is delimited by a marked groove in anterior view (Pandolfi & Tagliacozzo, 2015). TSR-36 differs from the McIII of *S. jeanvireti*, in the narrower antero-posteriorly medial part in proximal view, the more elongated transversally proximal articular surface, the flatter proximal border in anterior view, and the more reduced anterior and posterior articular surfaces in lateral view (Guérin & Tsoukala, 2013).

The dimensions of TSR-36 are close to *S. hemitoechus* from Lunel-Viel (France, Lacombat, 2005), Torre del Pagliacetto (Italy, Caloi & Palombo, 1978) and Grotte Lina (Italy, Pandolfi & Tagliacozzo, 2015) and *S. hundsheimensis* from Untermaßfeld (Germany, Kahlke, 2001) (Fig. 5). Most of the *S. etruscus* are smaller than the rest of *Stephanorhinus* species, however there is one specimen from Senèze (Se1756, France; Pandolfi et al., 2017) which is significantly larger and closer to the size of *S. jeanvireti* from Millia (Tsoukala, 2018).

Tibia. In distal view, the medial articular surface of the distal tibia TSR-50 (Fig. 3, g) is narrow and deep with prominent and rounded medial malleolus; the latter feature is not preserved in VOL-215 (Fig. 3, h). On the distal epiphysis of TSR-50, in distal view, the lateral articular surface is trapezoidal, less concave than the medial one, and transversally elongated, whereas in VOL-215 it is oval shaped and slightly concave. The posterior apophysis is quite prominent. In lateral view, only part of the fibula is attached to both specimens, not allowing the description of the distal articular surface; in VOL-215 the distal epiphysis in lateral view is high and flat though.

Remarks. VOL-215 and TSR-50 differ from *S. kirchbergensis* in the wider medial articular surface with limited antero-posterior development (Lobachev et al., 2021), character that is common with *S. etruscus* from Poggio Rosso (Italy, IGF-NHMF). VOL-215 and TSR-50 also differ from *S. hundsheimensis* because the tibia of latter taxon has a wider medial articular surface. Additionally, TSR-50 differs from *S. hundsheimensis* in the more prominent medial malleolus in distal view (Kahlke, 2001).

The dimensions of both distal epiphyses fall into the range of *S. etruscus.* The dimensions of TSR-50 fall into the range of the smaller specimens of *S. hundsheimensis* which however overlap with *S. etruscus* (Fig. 6).

Astragalus. In anterior view, the axis of the trochlea in APL-213 (Fig. 3i) has a faint inclination. There is a slight difference in height between the medial and lateral lips, which are parallel to each other. There is a depression between the trochlea and the distal articular surface, resulting in its

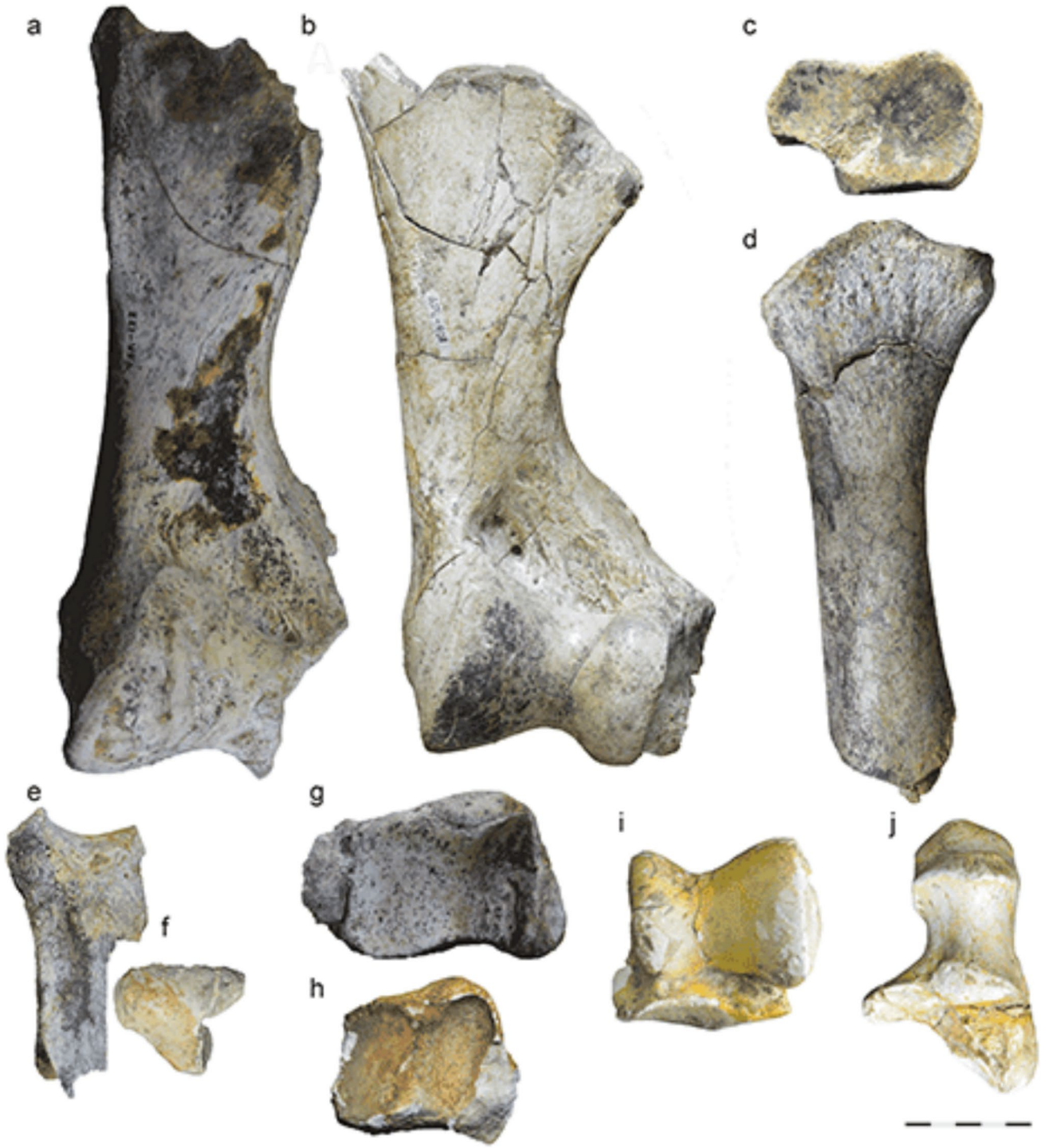

Fig. 3 *Stephanorhinus etruscus* from Tsiotra Vryssi (**a**, **c**–**g**), Volax (h) and Apollonia-1 (**b**, **i**, **j**). **a** Left humerus TSR-133; **b** left humerus APL-408; **c**, **d**, left radius TSR-C17-7; **e**, **f** right McIII TSR-36; **g** right tibia TSR-50; **h** right tibia VOL-215; **i** left astragalus APL-213 and **j** left calcaneus APL-213b. **a**, **b**, **d**, **e**, **i**: anterior view; **c**, **f**: proximal view; **g**, **h**: distal view; **j**: medial view. Scale bar equals 5 cm

higher location and clear distinction from the distal articular surface. In medial view, the medial tubercle is marked, rounded, slightly extending medially, and located in the middle of the medial face (SI Figure S3). In distal view, the medial articular surface is square- shaped, and almost flat. The lateral articular surface is irregular, generally like a half oval.

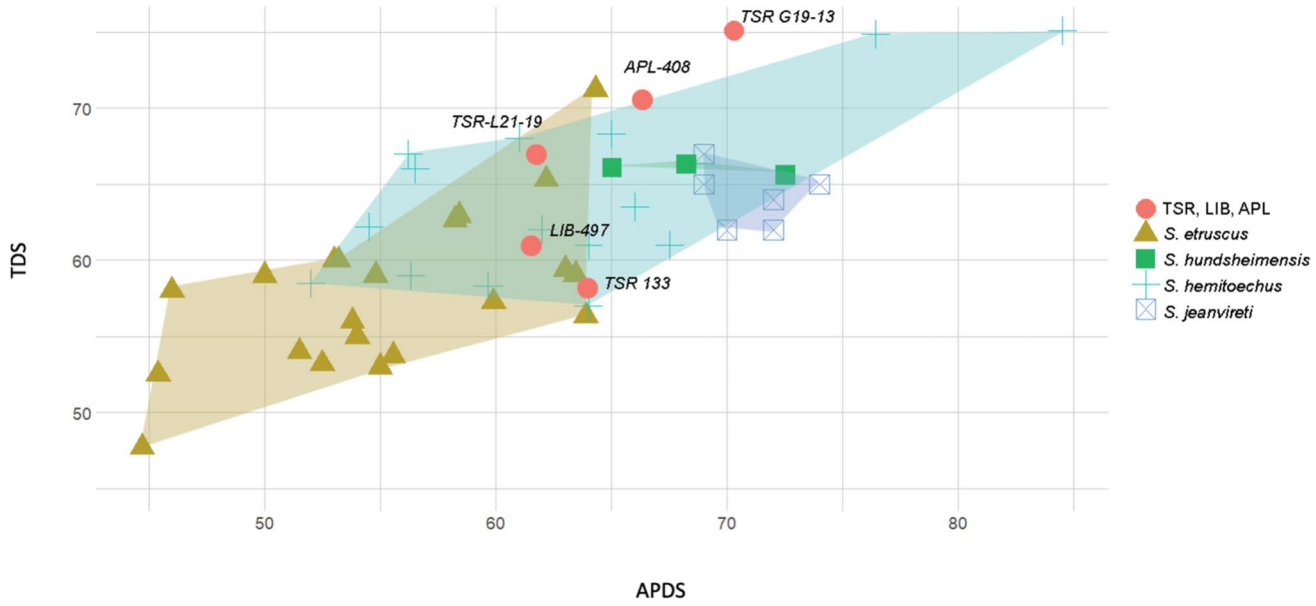

Fig. 4 Scatter plot comparing transversal diameter of the shaft (TDS) and antero-posterior diameter of the shaft (APDS) of the studied humeri specimens (in mm). Data from: Guérin and Heintz (1971); Guérin (1972, 2004); Mazza (1988); Mazza et al. (1993); Fortelius et al. (1993); Kahlke (2001); Lacombat (2005); Pandolfi and Petronio (2011); Pandolfi and Tagliacozzo (2015); Pandolfi et al. (2017); García-Fernández et al. (2023); Stefanelli et al. (2024)

Remarks. APL-231 differs from the astragalus of *S. hundsheimensis* in the more subtle inclination of the axis of the trochlea in anterior view, and in the oval shaped medio-distal articular surface in posterior view (Toula, 1902; Kahlke, 2001; García-Fernández et al., 2023). The astragalus of *S. jeanvireti* also differs from APL-231 by having a shallower groove of the trochlea in anterior view, with more medially protruding medial tuberosity, and a more convex medial border of the distal articulation in distal view (Lacombat & Mörs, 2008). Similarly, APL-213 differs from the astragalus of *S. hemitoechus* which shows a trochlea of less transversally developed in comparison with its height, as well as a shallower groove in anterior view and a less protruding medial tuberosity (Pandolfi & Tagliacozzo, 2015). Finally, APL-231 differs from the astragalus of *S. kirchbergensis* which has a stronger proximal protrusion of the medial lip in anterior view, a wider and higher depression located distally on the trochlea, and a narrower lateral lip in anterior view (Kahlke, 1975; Lobachev et al., 2021). APL-213 shares common characters with the specimens of *S. etruscus* from Upper Valdarno, such as the faint inclination of the axis of the trochlea in anterior view, the straight anterior border of the articular surface for the cuboid, the transversally elongated lateral lip in anterior view, and the oval shaped disto-medial articular surface in posterior view. The dimensions of APL-213 fall within the range of *S. etruscus* (Fig. 7).

Calcaneus. In lateral view, LIB-180 (SI Fig. S1) and APL-213b (Fig. 3j) have a straight posterior border. The difference in height between the most proximal part of the bone and the most anterior part of the *tuber calcanei* is small in LIB-180 but much greater in APL-213b. The beak and the *tuber calcanei* have the same width in LIB-180 while the width of the beak is slightly greater in APL-213b. In distal view the distal articular surface for the cuboid is rectangular-shaped in LIB-180 and almost rectangular-shaped in APL-213b.

Remarks: LIB-180 and APL-213b differ from those of *S. hundsheimensis*, in the higher most proximal part of the *tuber calcanei*, in the orientation of the anterior border of *tuber calcanei* in lateral view, as well as in the proximally convex posterior border of the bone in lateral view, and in the antero-posterior development of the beak and the *tuber calcanei* (Toula, 1902; Kahlke, 2001). They also differ from *S. jeanvireti*, in which the calcaneus shows a slightly convex and distally rounded shape of the *sustentaculum talii* (Pandolfi et al., 2019). The studied bones differ from *S. hemitoechus* which shows a straight posterior border of the bone in lateral view, with a faint concavity close to the distal part of the calcaneus (Pandolfi & Tagliacozzo, 2015; Tsoukala & Guérin, 2016). LIB-180 and APL-213b differ from *S. kirchbergensis* in the smaller difference in height between the most proximal part of the proximal tuberosity and the anterior part of the *tuber calcanei* (Kahlke, 1975). The calcaneus APL-213b shares common characters with that of *S. etruscus* from Upper Valdarno, Poggio Rosso and Olivola, such as the shape and size of the *tuber calcanei*, the rounded end of the *sustentaculum talii*, and the moderate

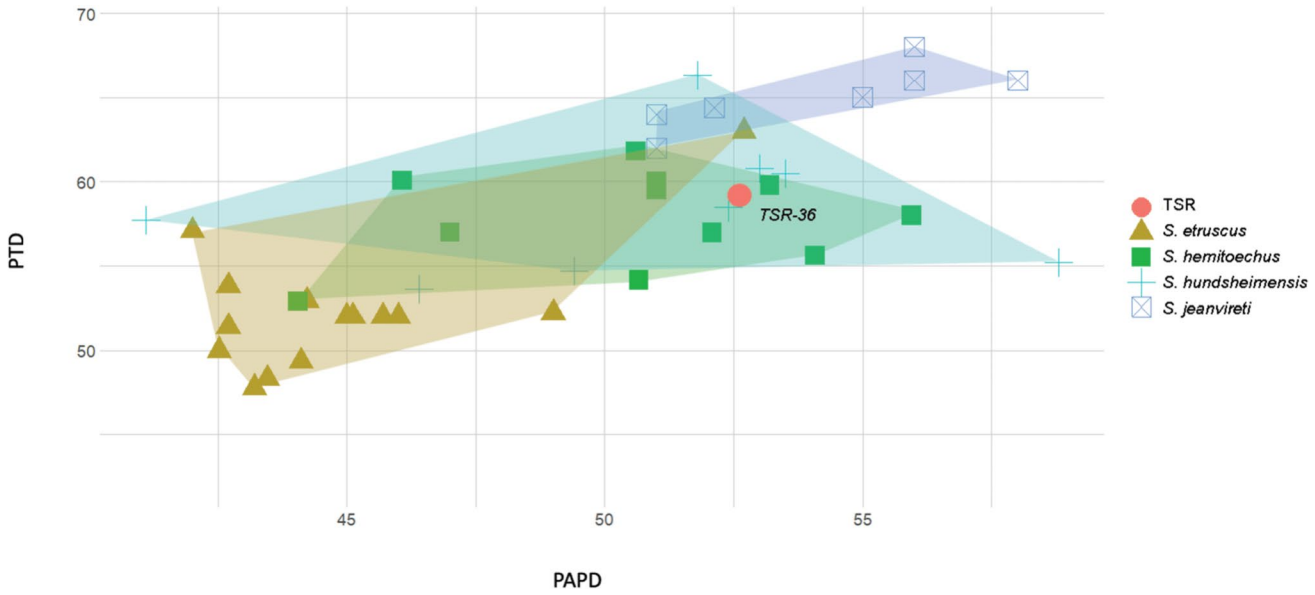

Fig. 5 Scatter plot comparing proximal transversal diameter (PTD) and proximal antero-posterior diameter (PAPD) of the McIII TSR-36 (in mm). Data from: Guérin and Heintz (1971); Guérin (1972, 1973); Caloi and Palombo (1978); Mazza (1988); Mazza et al. (1993); Cerdeño (1990), Fortelius et al. (1993), Kahlke (2001); Lacombat (2005); Guérin and Tsoukala (2013); Pandolfi and Tagliacozzo (2015); Pandolfi et al. (2017); García-Fernández et al. (2023); Stefanelli et al. (2024)

development of the *sustentaculum talii* in posterior view. Both APL-213b and LIB-180 share common characters with the previously mentioned samples of *S. etruscus* such as the straight posterior border in lateral view, and in the slightly greater width of the beak in comparison with that of *tuber calcanei* in lateral view.

Other tarsals. TSR-F18-64 includes the right tarsals (TSR-F18-64b, SI Fig. S7) and metatarsals (TSR-F18-64a, SI Fig. S8) of the same individual. In proximal view, the postero-medial tuberosity of the navicular is developed. The proximal articular surface for the astragalus is almost square with the antero-medial corner being very rounded and the postero-medial corner protruding posteriorly. There is not a great difference in height between the anterior and the posterior sides. In lateral view, the proximal border is concave. In medial view, the posterior tuberosity is moderately developed.

The cuboid is very polished and rather damaged. Its overall size is preserved, but in several places the spongy tissue is exposed. The distal articular surface for the MtIV is quite well preserved though. In anterior view, its shape is almost rectangular, with the lateral border higher than the medial one. In proximal view, the proximal articular surface for the astragalus and calcaneus has an almost trapezoidal shape with vertical and straight borders. In distal view, the articular surface for the MtIV is sub-circular shaped, but its borders are rather polished.

In lateral view, the first cuneiform is elongated with a small difference in width between the most proximal and the most distal part of the bone. At the proximal part, the articular surface is flat, rather subcircular and slightly elongated proximo-distally. In proximal view, the proximal articular surface for the navicular is triangular, flat, and occupies all the proximal face. In distal view, the articular surface for the MtII is kidney-shaped, being wider at the anterior part and extending towards the lateral.

In proximal view, the proximal articular surface of the second cuneiform is triangular, flat, and occupies all the proximal face. In medial view, only the tuberosity is preserved.

In anterior view, the anterior border of the third cuneiform, is convex and the medial border is straight. In proximal view, the articular surface for the navicular, which occupies this face is flat with a concavity running transversally. The posterior border is higher than the anterior one. In lateral view, there are three articular surfaces for the cuboid, of which the proximal one is transversally elongated. The anterior distal articular surface for the cuboid is larger than the posterior one, semicircular and elongated proximally. The posterior articular surface is circular, flat, and located more distally. In lateral view, the posterior border is larger than the anterior one, and there is a tuberosity at its proximal part. In anterior view, the outline is almost of a parallelogram, with the proximal border concave and the distal one slightly convex. In medial view, there is a strong concavity creating a vertical corner, whereas in the anterior part there is an

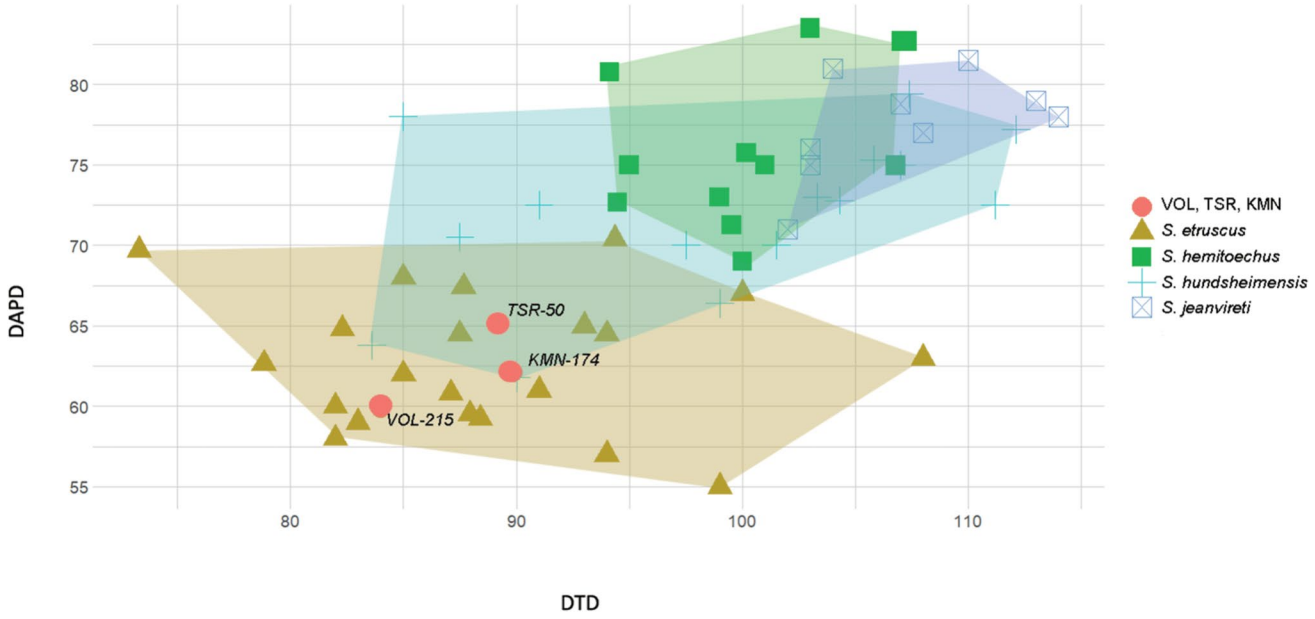

Fig. 6 The scatterplot of distal antero-posterior diameter (DAPD) and distal transversal diameter (DTD) of tibia TSR-50, KMN-174 and VOL-215 in mm. Comparative material from: Guérin and Heintz (1971); Guérin (1972, 2004); Mazza et al. (1993); Fortelius et al. (1993); Kahlke (2001); Lacombat (2005); Lacombat and Moullé (2005); Guérin and Tsoukala (2013); Pandolfi and Tagliacozzo (2015); Pandolfi et al. (2017); García-Fernández et al. (2023); Stefanelli et al. (2024)

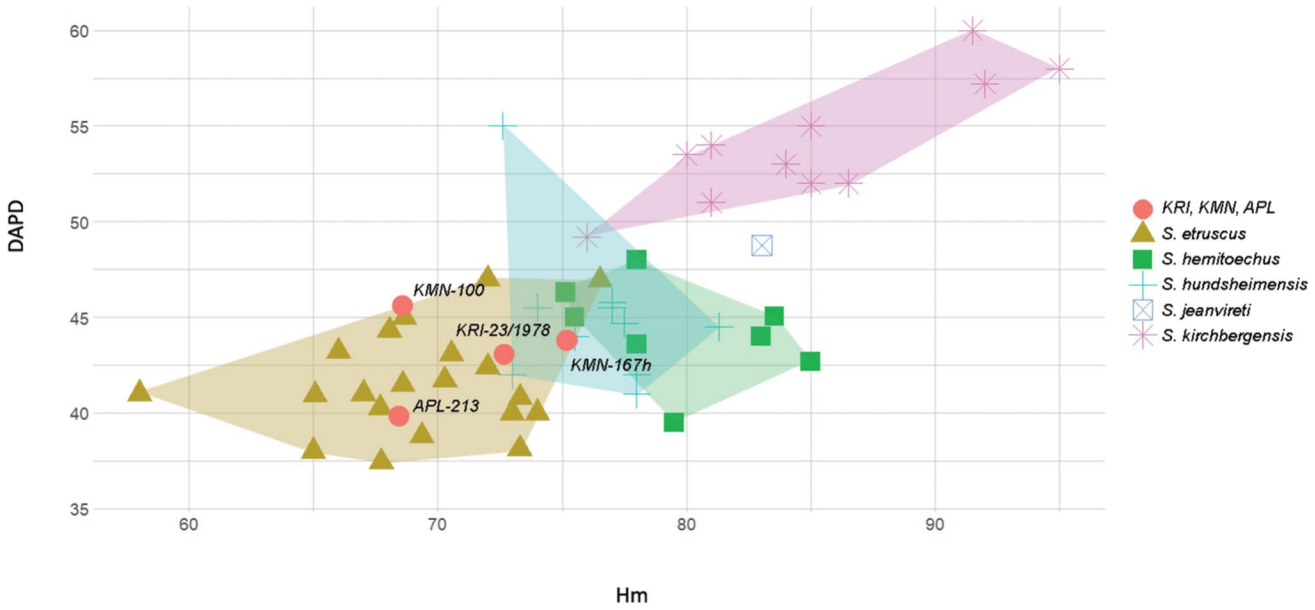

Fig. 7 The scatter plot of medial height (Hm) and distal antero-posterior diameter (DAPD) of the astragalus KMN-167h, KMN-100, KRI-23/1978 and APL-213. Data from: Guérin and Heintz (1971); Guérin (1972, 2004); Cerdeño (1990); Fortelius et al. (1993); Mazza et al. (1993); Kahlke (2001); Lacombat (2005); Lacombat and Mörs (2008); Guérin and Tsoukala (2013); Pandolfi and Tagliacozzo (2015); Pandolfi et al. (2017); García-Fernández et al. (2023)

articular surface of reduced circular shape and vertical to the distal articular surface.

Remarks. The navicular TSR-F18-64b differs from that of *S. hundsheimensis*, in the reduced medial extension of the anterior border (Pandolfi & Tagliacozzo, 2015), from *S. hemitoechus* in the strongly developed and more elongated

posterior tuberosity in medial view (Pandolfi & Tagliacozzo, 2015), and from *S. kirchbergensis* in the strongly concave medial border in proximal view, and the rather convex proximal border in medial view (Lobachev et al., 2021). It shares common characters with *S. etruscus* from Upper Valdarno, Olivola and Poggio Rosso, such as the straight medial border which bends towards the anterior border in proximal view.

The cuboid TSR-F18-64b resembles *S. etruscus* from Poggio Rosso, and *S. hemitoechus*; in that both, the medial and proximal borders are straight and perpendicular to each other, while the proximo-lateral corner is convex (Pandolfi & Tagliacozzo, 2015). In *S. jeanvireti* the medial border has a marked concavity, and the proximo-lateral corner creates a more acute angle (Guérin & Tsoukala, 2013). The cuboid of *S. hundsheimensis* is similar to that of *S. jeanvireti*, however the medial border is straight without any concavity (Kahlke, 2001).

The preservation of most of the tarsals is poor, however the cuboid TSR-F18-64a falls into the size variability of the smaller specimens of *S. etruscus* (Fig. 8). Nevertheless, *S. etruscus* shows great variation, especially in the maximal length and overlaps with all the specimens of *S. hundsheimensis* and with some specimens of *S. jeanvireti*.

The third cuneiform TSR-F18-56b differs from that of *S. hemitoechus* in the straight proximal border in anterior view (Pandolfi & Tagliacozzo, 2015). In anterior view, the proximal border of *S. hundsheimensis* is slightly more concave than that of *S. hemitoechus*. As well as its lateral part is slightly higher than the medial one, than in *S. hemitoechus* (Pandolfi & Tagliacozzo, 2015). However, the various specimens from Poggio Rosso, Olivola and Upper Valdarno show a great variability at the level of the concavity of the anterior border and in the maximal height of the bone. The specimen TSR-F18-56b shares common characters with *S. etruscus*, such as the concave proximal border in anterior view, the triangular shape of the articular face in proximal view, and the shape of the articular surfaces in lateral view (Italy, IGF-NHMF).

Metatarsals. In proximal view, the proximal articular surface for the second cuneiform of MtII TSR-F18-64a, APL-931 and APL-845 is moderately developed transversally, and of triangular shape. This surface is posteriorly delimited by a groove. In medial view, there is a relatively strong tuberosity close to the posterior border. In posterior view, the articular surface corresponding to the first cuneiform is flat and delimited by a groove. In lateral view, there are two articular surfaces for the MtIII and the third cuneiform respectively; the anterior one is located higher than the posterior in TSR-F18-64b, however they are at the same level in APL-931 and APL-845. The anterior articular surface is not in contact with the proximal articular surface for the second cuneiform, slightly protruding and quite damaged at the proximal part in TSR-F18-64b.

In proximal view, the epiphysis of MtIII TSR-F18-64a, is occupied by the triangularly shaped proximal articular surface for the third cuneiform. The antero-lateral corner is protruding laterally with a slight concavity at the medial border. The anterior border is strongly convex with a slight medial concavity. In anterior view, the proximal border is almost straight and oblique, presenting a strong difference in height between the medial and the lateral corners. In lateral view, there are two articular surfaces for the articulation with the MtIV. The anterior one is in contact with the proximal articular surface, trapezoidal shaped, flat, and parallel oriented compared with the sagittal plane. The posterior articular surface is clearly distinguished from the proximal articular surface for the second cuneiform through a relatively wide groove; it has almost rounded shape, flat and strongly angled (~ 30°) compared to the proximo-distal axis. The section of the diaphysis is elliptical shaped with convex anterior and posterior borders.

The proximal articular surface for the cuboid of MtIV TSR-F18-64a is sub-squared, flat with a slight antero-posterior concavity. In medial view, there are two articular surfaces for the MtIII; the anterior one is slightly higher than the posterior, more elongated and oval shaped. The posterior articular surface is sub-circular, flat and protrudes from the corpus of the bone. In anterior view, the proximal border is straight with a minor concavity; the lateral border is quite damaged. The section of the preserved diaphysis is trapezoidal-like with rounded corners.

Remarks. The MtII TSR-F18-64a, APL-931 and APL-845 share common characters with *S. etruscus* from Olivola, Upper Valdarno, Poggio Rosso and Pirro Nord, such as the elongated transversally proximal articular surface for the second cuneiform with moderate antero-posterior development, the moderate difference in height of the articular surfaces in lateral view, and the concave proximal border in anterior view. They differ from *S. hundsheimensis* in the weaker antero-posterior development of the proximal articular surface (Pandolfi & Tagliacozzo, 2015), and from *S. hemitoechus* in the straighter proximal border in anterior view and the wider groove separating the two articular surfaces in lateral view (Pandolfi & Tagliacozzo, 2015). All studied specimens differ from *S. jeanvireti* in the much higher location of the anterior articular surface in comparison with the posterior one in lateral view and in the stronger anterior tuberosity (Pandolfi et al., 2019). In addition, they differ from *S. kirchbergensis* in the much wider articular surface in proximal view, with a marked antero-posterior concavity (Pandolfi & Tagliacozzo, 2015; Lobachev et al., 2021). The dimensions of the proximal epiphysis of TSR-F18-64a are much smaller than *S. etruscus*, contrary to those

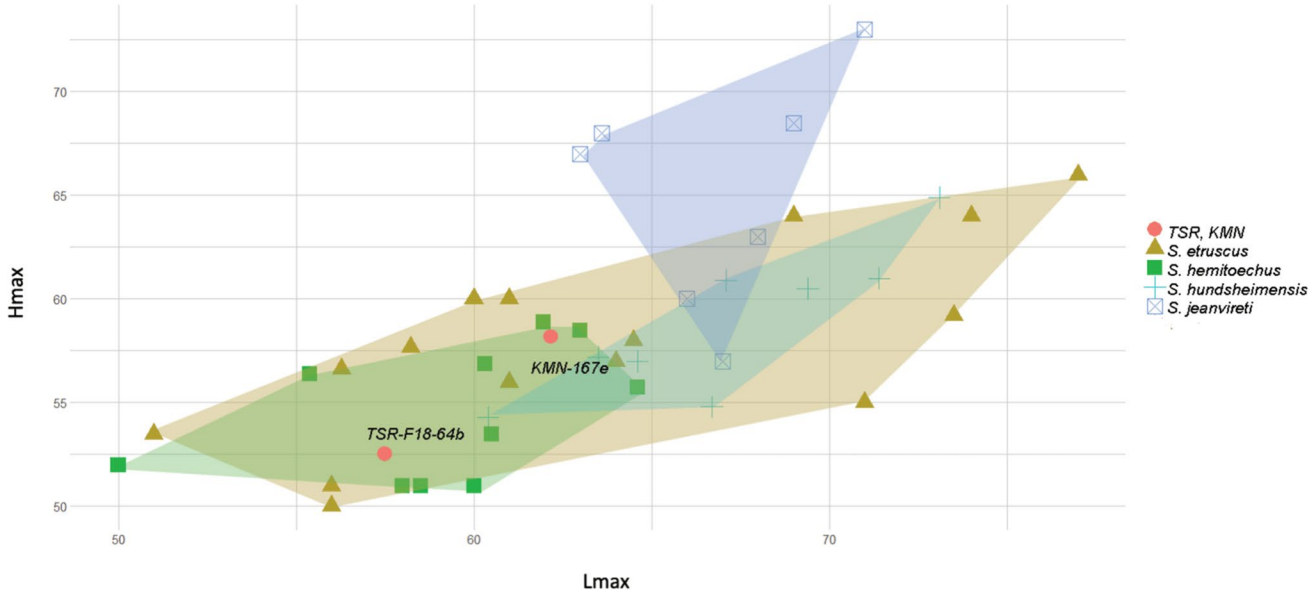

Fig. 8 The scatter plot of the maximal height (Hmax) and the maximal length (Lmax) of the cuboids TSR-F18-64a and KMN-167a in mm. Comparative material from: Guérin and Heintz (1971); Guérin (1972, 1973); Cerdeño (1990); Fortelius et al. (1993); Kahlke (2001); Lacombat (2005); Guérin and Tsoukala (2013); Pandolfi and Tagliacozzo (2015); Pandolfi et al. (2017); García-Fernández et al. (2023)

of APL-931 and APL-845 which fall into the range of *S. etruscus* (Fig. 9).

The straight and inclined proximal border in anterior view of the MtIII TSR-F18-64a, and the convex anterior border with a slight concavity at the medial part in proximal view, are features shared with *S. etruscus* from Upper Valdarno, Poggio Rosso and Olivola. However, in *S. etruscus* the proximal border may be more concave. TSR-F18-64a differs from *S. hemitoechus*, in the strongly concave anterior border with more transversally developed anterior part in proximal view, less inclined proximal border in anterior view, and greater difference in height between the two articular surfaces in lateral view (Pandolfi & Tagliacozzo, 2015). It is also different from *S. kirchbergensis*, in the much greater difference in height between the two articular surfaces and the subelliptical posterior articular surface in lateral view (Kahlke, 1975), and from *S. jeanvireti*, in the less inclined proximal border in anterior view and the greater difference in height of the articular surfaces in lateral view (Guérin & Tsoukala, 2013; Pandolfi et al., 2019).

The MtIV TSR-F18-64a differs from that of *S. kirchbergensis*, in the triangular shaped proximal articular surface in proximal view and the more elongated, oval-shaped articular surfaces in posterior view (Pandolfi & Tagliacozzo, 2015; Lobachev et al., 2021). No differences between *S. jeanvireti*, *S. etruscus* and *S. hemitoechus* have been observed. *Stephanorhinus hundsheimensis* may have a squarer articular surface but the comparison is based only on drawings (Kahlke, 2001; Guérin & Tsoukala, 2013; Pandolfi & Tagliacozzo, 2015; Pandolfi et al., 2019). The size of proximal epiphysis of MtIV TSR-F18-64a (Fig. 10) is within the variability of *S. etruscus* and close to a specimen of *S. hundsheimensis* from Untermaßfeld (Germany, Kahlke, 2001).

Stephanorhinus cf. ***S. hundsheimensis*** (Toula, 1902)

Material. Cranium, KMN-1; humerus, TSR-G19-13, TSR-L21-19; proximal epiphysis of ulna, RIZ-27a; proximal epiphysis of radius, RIZ-27b; femur, TSR-F18-56; diaphysis of femur, TSR-G20-50, TSR-D16-27, TSR-F22-3, TSR-F8-81, KMN-98; distal epiphysis of tibia, KMN-174; astragalus, KMN-167h; calcaneus, KMN-167i; navicular, KMN-167g; cuboid, KMN-167e; first cuneiform, KMN-167f; second cuneiform, KMN-167k, third cuneiform, KMN-167d; MtII, KMN-167c; MtIII, KMN-167b; MtIV, KMN-167a, TSR-G16-41.

Descriptions and comparisons. **Cranium.** KMN-1 is an almost complete juvenile cranium moderately preserved. The specimen shows strong damages at the parietal, basicranial and right-side parts, and a neurocranial portion twisted to the left side (Fig. 11). There are no teeth preserved apart from a non-erupted either DP4 or P4. Regularly the sutures are not visible due to preservation, although there are some exceptions that will be noted. In dorsal view, the nasal bones are wide caudally becoming rather abruptly narrower toward their rostral tip; their length is ca. 183 mm. Close to the nasal tip there is a small elliptical rugosity, probably corresponding to a horn boss. The ventral surface of the nasals is flattened. The fronto-nasal suture can be observed in dorsal

view; it is placed slightly in front of the anterior level of the orbits. In lateral view, the top profile of the nasals is flat caudally but slightly convex to the front and bends downwards in front of the horn boss imprint. Nasal septum is not developed. Most of the maxillary is damaged. The contact of the lacrimal bone and the nasal is not visible, and the lacrimal tubercle (preorbital process) is quite damaged but moderately developed. The widest part of the frontal bone is at the supra-orbital part. The dorsal surface of the frontals is flat, sub horizonal and slightly raising towards the parietal. Just behind the fronto-nasal suture there is a small, rounded boss, likely representing the place of a second horn. The braincase is rectangle in dorsal view. The parietal is elongated (from the rostral tip of nasal to the highest point of occiput: 582 mm; rostral tip of nasals to occipital condyles: 538 mm, maximal width at the level of the zygomatic arches: 124 mm), and narrow. The temporal lines are weak but visible and run subparallel to each other. The parietal-interparietal suture is preserved in dorsal view. In occipital view, the sutures between the occipital and the mastoid (of the right preserved side, the left one is partly destroyed and filled with cement) are preserved. The occiput is high. The upper part of the occiput is badly preserved, but its overall outline is trapezoidal, with the broadest part at the level of the mastoids. The nuchal crest is severely damaged but rather rounded in posterior view and protruding posterodorsally. The postglenoid process and the sphenoid region are not preserved. The external auditory pseudomeatus is ventrally closed, quite large and rounded.

Remarks. The Eurasian Pleistocene juvenile rhino material is very limited, and it is no possible to compare specimens with same estimated age. Only two juvenile *Stephanorhinus* crania are figured and described, *S. kirchbergensis* from China (Tong & Wu, 2010) and *S. hundsheimensis* from Cova del Rinoceront, Spain (García-Fernández et al., 2023). In addition, young crania of *Coelodonta* are known for *C. nihowanensis* from China and *C. antiquitatis* from Siberia (Tong & Wang, 2014; Protopopov et al., 2015; Iurino et al., 2020). There is also a specimen from Melpignano (Italy) with limited distinguished morphological characters, resulting in its assignment as Rhinocerotinae indet. (Iurino et al., 2020) but probably belonging to *S. hemitoechus*, a species well-documented in that site (Pandolfi & Petronio, 2011). Unfortunately, *S. hundsheimensis* juvenile cranium #8261 from Spain (García-Fernández et al., 2023) is not complete and its conservation is poor precluding further comparison. Iurino et al. (2020) suggested that the juvenile crania of *Coelodonta* are characterized by a flatter fronto-parietal profile than that of *S. kirchbergensis*. In the latter one, the fronto-parietal profile creates an angle. In KMN-1, the parietal has a flat profile, but the specimen is seriously damaged near the frontal. The parietal and the jugal (zygomatic arch) are running parallel in KMN-1, in difference from *S. kirchbergensis* No. H36 cranium where it forms an acute angle (Tong & Wu, 2010, Fig. 11A). In KMN-1 the lateral profile of the occipital crest is triangular with a narrow vertex, like in the specimen from Melpignano, and the two juvenile *Coelodonta* specimens, and in difference with *S. kirchbergensis,*

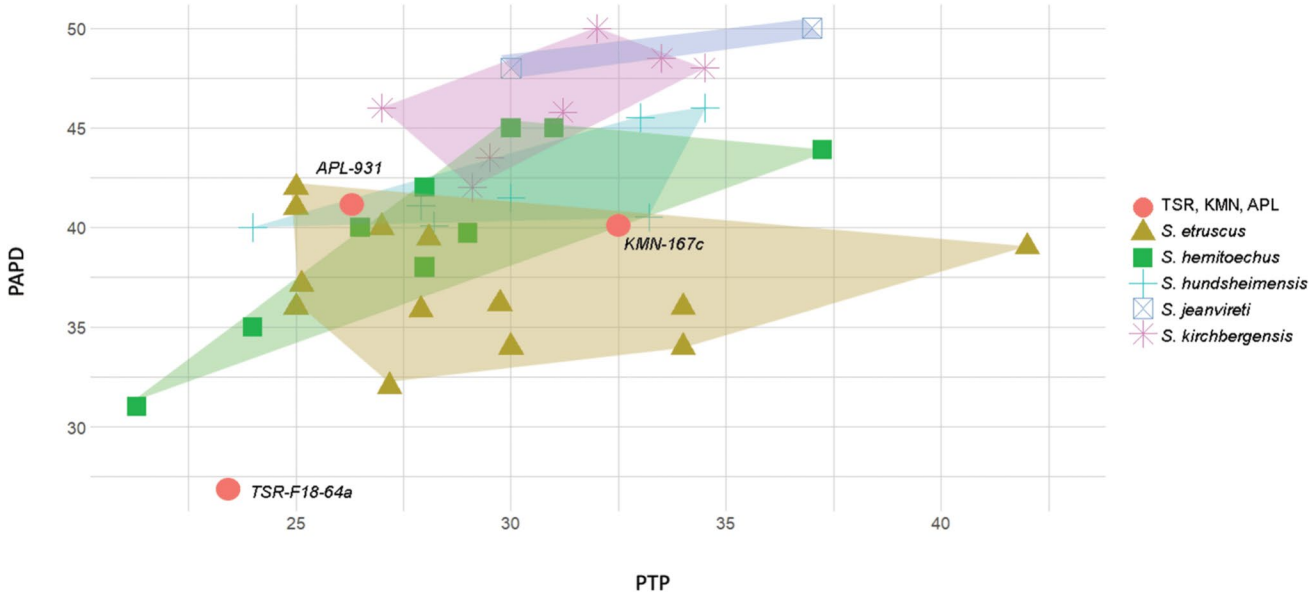

Fig. 9 The scatter plot of the proximal antero-posterior diameter (PAPD) and the proximal transversal diameter (PTP) of the MtII TSR-F18-64a, KMN-167c and APL-931 in mm. Comparative material from: Guérin and Heintz (1971); Guérin (1972, 1973); Caloi and Palombo (1978); Cerdeño (1990); Fortelius et al. (1993); Kahlke (2001); Pandolfi and Tagliacozzo (2015); Pandolfi et al. (2017); García-Fernández et al. (2023)

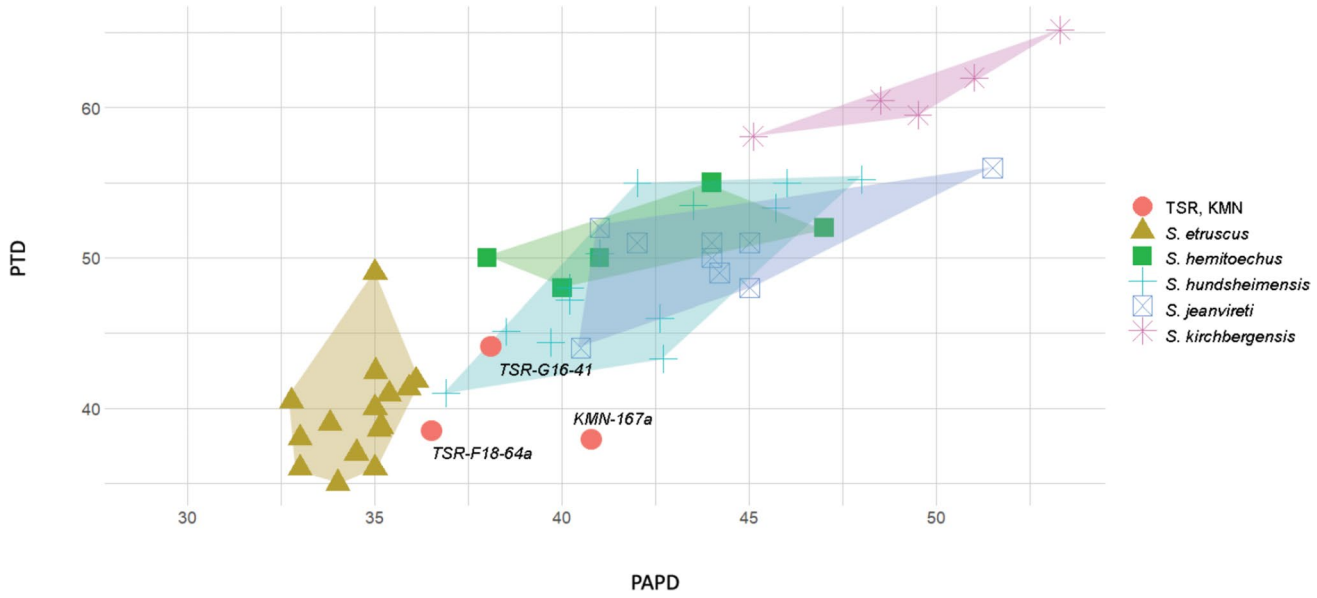

Fig. 10 The scatter plot of the proximal transversal diameter (PTD) and the proximal antero-posterior diameter (PAPD) of the MtIV TSR-G16-41, TSR-F18-64a and KMN-167a in mm. Comparative material from: Guérin and Heintz (1971); Guérin (1972); Fortelius et al. (1993); Kahlke (2001); Lacombat (2005); Guérin and Tsoukala (2013); Pandolfi et al. (2017); García-Fernández et al. (2023)

in which the occipital crest is rounded and more dorso-ventrally developed (Iurino et al., 2020). Comparing the external auditory pseudomeatus, in KMN-1 it is quite broad and circular shaped, in difference from the drop-shaped meatus of *S. kirchbergensis* which is also placed closer to the occipital plane (Iurino et al., 2020). Finally, compared to a juvenile *S. etruscus* from Senèze (France; NMB), KMN-1 differs at the great length, concave dorsal profile, and the narrow and arched nasals. These characters distinguish the studied specimen from *S. etruscus*, resulting, confidently, in its attribution to *S. hundsheimensis*.

Humerus. The articular heads of TSR-G19-13 and TSR-L21-19 (Fig. 12l, m) are rounded and extend posteriorly, in proximal view; the greater tubercle extend more laterally than proximally in anterior view and the bicipital groove is wide and concave on both specimens, but on TSR-L21-19 it is more concave at the lateral part. In both specimens, the medial lip of the trochlea is more transversally extended in anterior view. In posterior view, the olecranon fossa is high with an elliptic outline. The lateral epicondyle is distally and laterally protruding, though more in TSR-G19-13. The epicondylar crest is moderately developed and both distal epiphysis and trochlea are oblique. In distal view, the lateral border of the distal trochlea is slightly concave in TSR-G19-13 and undulated in TSR-L21-19.

Remarks. TSR-G19-13 and TSR-L21-19 share common characters with *S. hundsheimensis*, such as the high and elliptical-shaped olecranon fossa in posterior view; the more laterally than proximally extended greater tubercle, and in the more extended transversally medial lip of the trochlea (García-Fernández et al., 2023; Stefanelli et al., 2024). Both TSR-G19-13 and TSR-L21-19 differ from APL-408 of *S. etruscus* in which the shape of the olecranon fossa is triangular, wide and deep. They both differ from *S. jeanvireti* in the more oblique trochlea in anterior view, compared to the straight trochlea of *S. jeanvireti* from Riano (Pandolfi, 2011). They also differ from *S. kirchbergensis* mainly in the very wide olecranon fossa in posterior view (Guérin, 1980).

Radius and ulna. The trochlear notch of the ulna RIZ-27a (Fig. 12k) is robust and asymmetrical. In anterior view, the medial articular surface is parallel to the medial border of the diaphysis, creating a ~ 45° angle with the lateral articular surface. The articular surfaces for the radius are flat, rectangular shaped, with the lateral one being wider. In lateral view, the preserved part of the olecranon is antero-posteriorly wide and robust. The anconeal process moderately projects forwards and is perpendicular to the corpus of the bone. The preserved diaphysis has a triangular cross section.

In proximal view, the medial articular surface of the radius RIZ-27b (Fig. 12i, j) is slightly concave, sub-squared in shape with curved but damaged medial outline. The lateral articular surface is much smaller and more concave than the medial one. The postero-lateral border is oblique and slightly concave; it forms a ~ 120° angle with the posterior border of the articulation. In anterior view, the proximal border of the lateral articular surface is reduced and concave with a small difference in height between the medial and the lateral

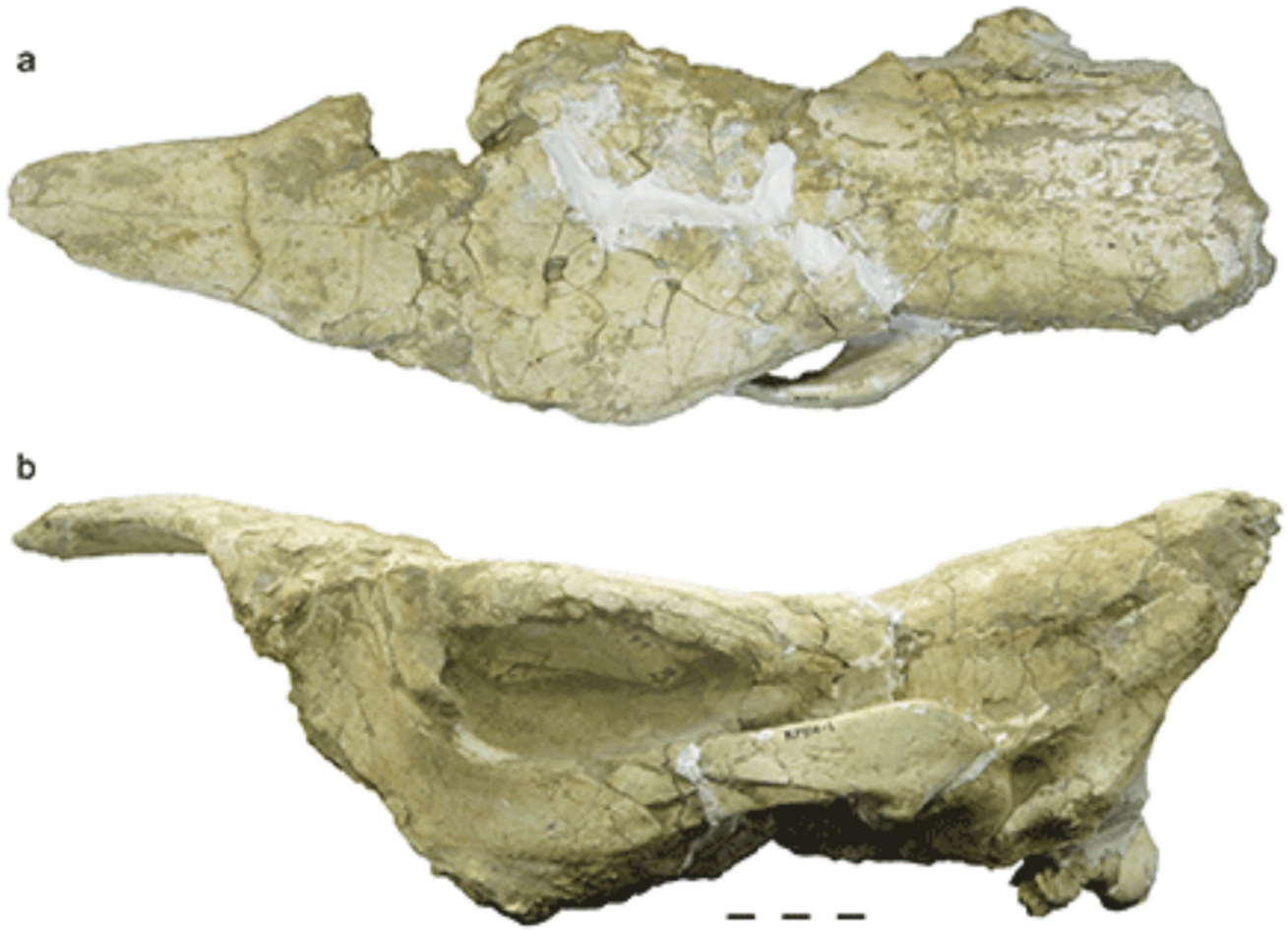

Fig. 11 The juvenile cranium of *Stephanorhinus* cf. *S. hundsheimensis* (KMN-1) from Krimni-3, in dorsal (**a**) and lateral (**b**) views. Scale 50 mm

articular surfaces. The *brachii biceps* is slightly developed. In posterior view, the lateral articular surface is large, half-circle shaped whereas the medial one is not preserved. In distal view, the articular surface is asymmetrical. The medial part of the articulation is concave at the anterior side, and convex at the posterior. The lateral part is moderately concave. The posterior convexity of the articular surface for the scaphoid is small; and the lateral border is slightly concave. In anterior view, the styloid apophysis is well developed and protruding. At the lateral part of the epiphysis there is a very strong tuberosity making the transversal diameter of the distal epiphysis much greater than that of the articulation.

Remarks. The radius RIZ-27b shares common characters with *S. hundsheimensis* such as the protruding styloid apophysis (Kahlke, 2001). However, it differs mainly in the straight anterior border of the articulation in proximal view, and the very wide angle (almost 180°) of the posterior border. It also differs from *S. hemitoechus* from Valle Radice (Sora, Italy), in the more acute posterior angle of the articulation in proximal view, the stronger posterior process in anterior view, and the difference in height between the lateral articular surface (for the semilunar) and the styloid apophysis (Pandolfi & Tagliacozzo, 2015). RIZ-27b differs from *S. jeanvireti* from Milia (Greece), as in the later the lateral articular surface of the proximal epiphysis extends outwards in anterior view (Tsoukala, 2018). It also differs from *S. kirchbergensis* from Siberia, in the straight posterolateral border in proximal view, the straight anterior border of the articulation and the straight proximal border in anterior view (Lobachev et al., 2021). RIZ-27b differs from APL-278 of *S. etruscus* in having a proportionally larger proximal lateral articular surface, with a more convex anterior border. Additionally, in anterior view, RIZ-27b has a less concave lateral-proximal border, a reduced and more medially placed *brachii biceps* and a stronger, more distally placed lateral tuberosity. In comparison with the TSR radii of *S. etruscus*, RIZ-27b is very similar to TSR-C17-7, but differs at the less concave, though slightly damaged, lateral border in anterior view, and the stronger lateral tuberosity in the proximal epiphysis. The specimen TSR-G21-72 differs from RIZ-27b, since in proximal view the latter has a less

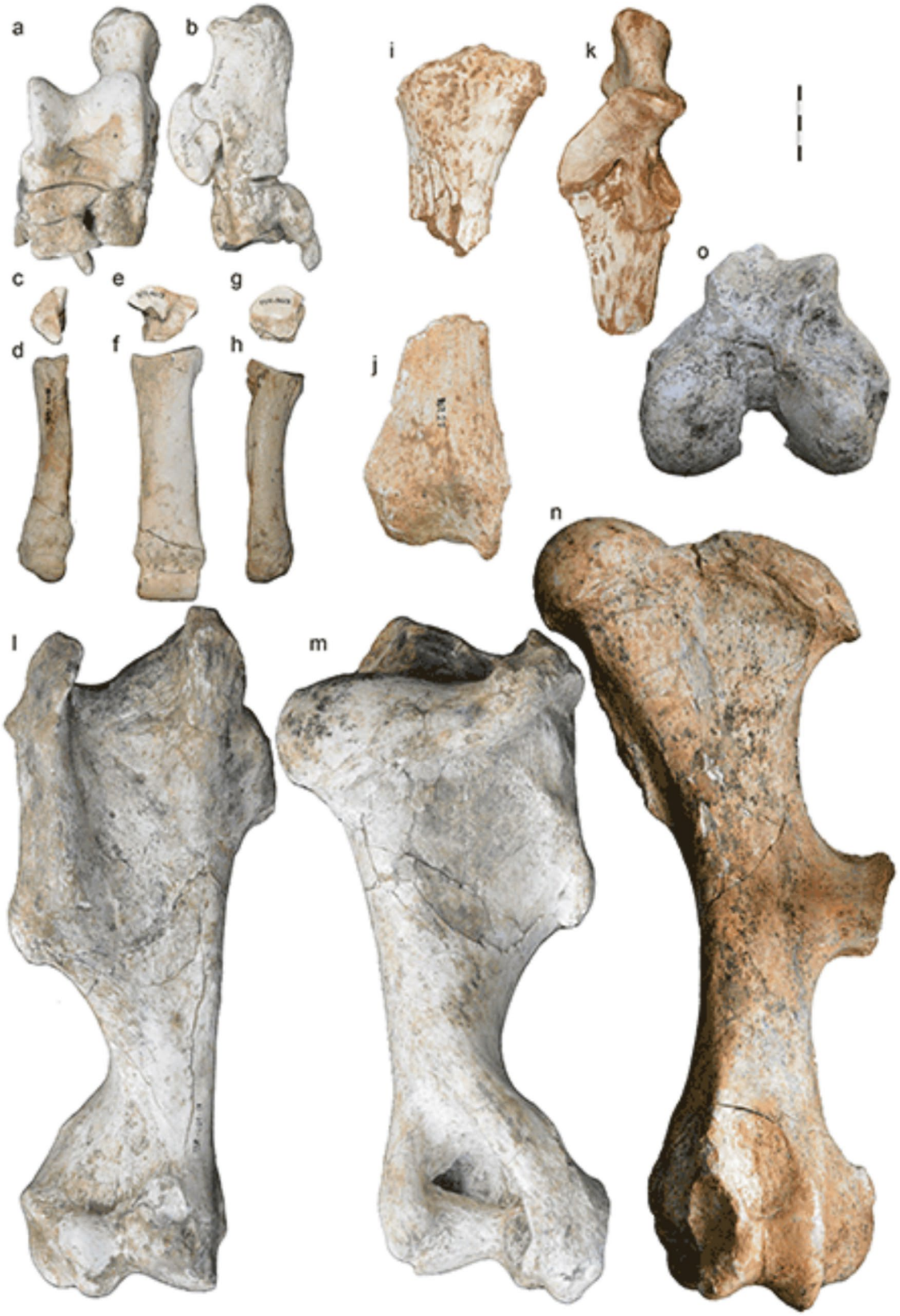
a
b
i
k
c
e
g
d
f
h
j
o
n
l
m

◂**Fig. 12** *Stephanorhinus* cf. *S. hundsheimensis* from Krimni-3 (**a–h**), Riza-1 (**i–k**) and Tsiotra Vryssi (**l–o**). **a**, **b**, left tarsals KMN-167 (astragalus: KMN-167h, calcaneus: KMN-167i, navicular: KMN-167g, cuboid: KMN-167e, first cuneiform: KMN-167f, second cuneiform: KMN-167k, third cuneiform: KMN-167d); **c**, **d** MtII KMN-167c; **e**, **f**, MtIII KMN-167b; **g**, **h** MtIV KMN-17a; **i**, **j**, left radius RIZ-27a; **k** left ulna RIZ-27; **l**, **m** right humerus TSR-L21-19; **n**, **o** left femur TSR-F18-56. **a**, **d**, **f**, **h**, **i**, **j**, **k**, **l**: anterior view; **c**, **e**, **g**: proximal view; **o**: distal view; **b**: lateral view. Scale bar equals 5 cm

concave lateral articular surface. Moreover, in anterior view, it is stockier, has a less wide lateral-proximal border, and a reduced *brachii biceps*.

Femur. In proximal view, the shape of the femoral head of TSR-F18-56 (Fig. 12n, o) is rounded, and slightly transversally elongated. It has a clear ligament fossa located at the posterior and medial part. The neck is narrow. The great trochanter has its top slightly damaged, however it appears moderately extended with a marked great trochanter convexity. The third trochanter is slightly enlarged outward, broken at the lateral part, and located at the middle of the diaphysis. The blunt lesser trochanter is extended until the height of the third trochanter. The distal epiphysis is strongly asymmetrical in distal view. The medial trochlear ridge is damaged, and the difference in height with the lateral one is not traceable; they form an angle of about 90°. The medial epicondyle is as developed as the lateral one; the medial condyle though is more robust, rounded and twice as wide as the lateral one. The intercondylar fossa is moderately developed. TSR-G20-50, TSR-D16-7, TSR-F8-81 and TSR-F22-3, and KMN-98 preserve only the diaphysis of the femur which are quite robust.

Remarks. TSR-F18-56, which is the best preserved and most complete femur, shares common characters with *S. hundsheimensis*, such as the trapezoidal shape of the third trochanter, the asymmetrical trochlea, the clearly larger medial lip of the trochlea than the lateral lip, and the wideness of the intercondylar fossa (García-Fernández et al., 2023; Stefanelli et al., 2024). These characters also differentiate TSR-F18-56 from *S. etruscus.* It differs from *S. jeanvireti*, in the shape of the condyles in distal view, which are highly asymmetrical with the lateral one protruding distally (Guérin, 1972).

The dimensions of the diaphysis show that the specimens TSR-F18-56, TSR-D16-27, TSR-F22-3 and TSR-G20-50, TSR-F8-81 and KMN-98 fall clearly into the range of *S. hundsheimensis* (Fig. 13).

Tibia. The distal epiphysis of the tibia KMN-174 (SI Fig. S10) is quite robust with the distal epiphysis of the fibula attached. In distal view, the medial articular surface is concave, narrow and elongated, with a rounded and prominent medial malleolus. In the same view, the lateral articular surface is trapezoidal shaped.

Remarks. KMN-174 differs from *S. etruscus* (including TSR-50 and VOL-215) in the more concave lateral articular surface in distal view. Additionally, it is more robust, and the dimensions of the distal epiphysis fall into the size range of *S. etruscus* which overlaps with the smaller sized specimens of *S. hundsheimensis*. The size of KMN-174 is similar to *S. hundsheimensis* (#8096) from Cova del Rinoceront (Fig. 6).

Astragalus. The axis of the astragalar trochlea of KMN-167h (Fig. 12a, b), in anterior view, is inclined; it preserves a broad trochanter and a wide lateral lip of the trochlea, in anterior view.

Remarks. KMN-167h is articulated with the other tarsals, allowing the comparison only of the anterior view, in which the axis of the trochlea is inclined, a common character with *S. hundsheimensis* (Toula, 1902; Kahlke, 2001). Its dimensions fall into the range of the larger specimens of *S. etruscus* and the smaller specimens of *S. hundsheimensis* (Fig. 7).

Calcaneus. In the calcaneus KMN-167i (Fig. 12a, b), the difference in height between the most proximal part of the *tuber calcanei* and its anterior point is great. The beak has the same width as the *tuber calcanei* and the posterior border of the bone, in lateral view, is slightly convex close to the proximal part.

Remarks. KMN-167i shares common characters with *S. hundsheimensis*, including the sightly convex close to the proximal part posterior border in lateral view, and in the similarly wide beak and *tuber calcanei* (Toula, 1902; Kahlke, 2001), characters that differentiate it also from APL-213b and LIB-180 of *S. etruscus*.

Other tarsals. Only the anterior and medial sides of the navicular KMN-167g are preserved. In anterior view, the outline of the bone is trapezoidal. The proximal border is convex, the distal sinuous, the medial straight and the lateral creates an acute angle with the proximal border. In medial view, there is a strong tuberosity occupying most of the medial face.

The shape of the cuboid KMN-167e, in anterior view, is rectangular with the lateral border being higher than the medial one. In distal view, the articular surface for the MtIV is triangular shaped with a medial border concave distally.

The first cuneiform KMN-167f (Fig. 12a, b) is elongated with its distal part narrower than the proximal one. The second cuneiform (small cuneiform) KMN-167k is square shaped in medial view.

The outline of the third cuneiform KMN-167d (Fig. 12a, b) is almost rectangular in anterior view. The anterior border is convex, and the medial one is almost straight in anterior view. In distal view, it has a triangular outline with a concave lateral border and a straight anterior one.

Remarks. The navicular KMN-167g differs from TSR-F18-64b of *S. etruscus* in the more pronounced proximo-lateral extension. Similarly, the cuboid KMN-167e differs from the cuboid TSR-F18-64b in the more prominent postero-distal extension in lateral view and the general robustness (Fig. 8). The first cuneiform of KMN-167f is more elongated and robust than TSR-F18-64b. The third cuneiform KMN-167d is similar with *S. hundsheimensis* from Cova del Rinoceront (individual #8096) especially in the more concave lateral border in distal view (García-Fernández et al., 2023). The same border is less concave in TSR-F18-64b.

Metatarsals. The proximal articular surface for the second cuneiform of MtII KMN-167c (Fig. 12c, d) is damaged in the posterior part. In anterior view, the proximal border is concave, the body is curved and displays a tuberosity close to the distal epiphysis which occupies the anterior and extends to the medial side. In proximo-medial view, the anterior articular surface for the MtIII is placed higher than the posterior one. The former is oval shaped, while the latter is broken in the proximal part, resulting in a more triangular shape.

In proximal view, the epiphysis of MtIII KMN-167b (Fig. 12e, f) has a triangular shaped articular surface for the 3rd cuneiform. The anterior border is sinuous and the lateral border strongly concave. In anterior view, the proximal border is concave medially. In lateral view, the anterior articular surface is clearly higher than the posterior one, both rounded in shape. In medial view, the two articular facets for the MtII are close to each other. Both have a semi-circular shape, with the anterior being smaller than the posterior one.

In proximal view, the articular surface for the cuboid of MtIV TSR-G16-41 is elliptical with an irregular anterior border. The medial border is straight near the anterior part, forming an obtuse angle. The posterior border of the proximal articular surface is convex. In both TSR-G16-41 and KMN-167a (Fig. 12g, h), in proximal view, there is a deep and a narrow groove that separates the proximal articular surface from the strong lateral tuberosity. In medial view, there are two articular surfaces for the MtIII, the posterior one is eye-shaped and flat, protruding posteriorly and being separated from the proximal articular surface. In medial view, in TSR-G16-41, the anterior articular surface is trapezoidal shaped and located higher than the posterior one; the two articular surfaces are separated from each other by a rather deep and wide groove. In KMN-167a the two articular surfaces are smaller than in TSR-G16-41 and the groove separating them is narrower. The cross section of the preserved diaphysis of both specimens is circular.

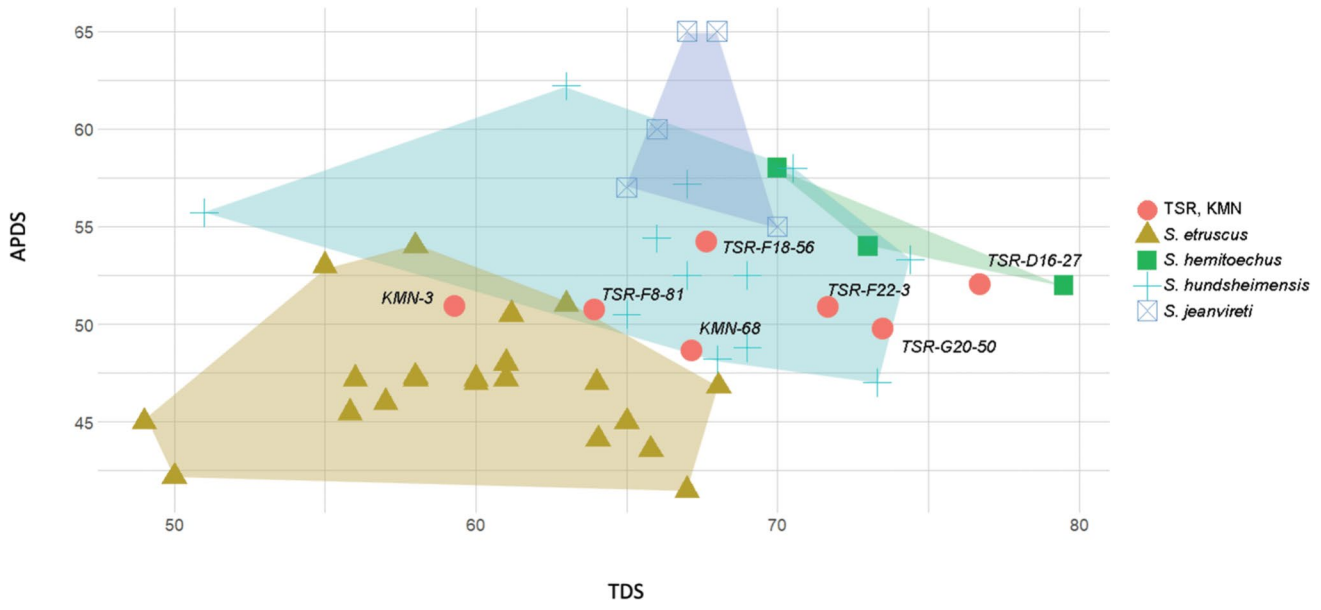

Fig. 13 Scatter plot of the antero-posterior diameter of the shaft (APDS) and the transversal diameter of the shaft (TDS) of the diaphysis of the femur distally to the third trochanter of TSR-F8-81, TSR-F18-56, TSR-F22-3, TSR-G20-50, TSR-D16-27, KMN-68 and KMN-3, in mm. Comparative material from: Guérin and Heintz (1971); Guérin (1972, 2004); Fortelius et al. (1993); Mazza et al. (1993); Kahlke (2001); Tsoukala and Guérin (2016); Pandolfi et al. (2017); García-Fernández et al. (2023), Stefanelli et al. (2024)

Remarks. The dimensions of the proximal epiphysis of MtII KMN-167c fall into the range of both *S. hundsheimensis* and *S. etruscus* (Fig. 9). MtIII KMN-167b shares common characters with *S. hundsheimensis* in the almost horizontal proximal border in anterior view, and the less transversally developed proximal articular surface, in proximal view (Kahlke, 2001; García-Fernández et al., 2023). These characters are not observable on TSR-F18-64a that instead shows a concave medially proximal border in anterior view, and in proximal view, more transversally developed proximal articular surface with less concave medial border and more concave anterior border.

The MtIV TSR-G16-41 and KMN-167a differ from TSR-F18-64a, assigned to *S. etruscus,* in the shape of the proximal articular surface. The transversal diameter of the proximal articular surface of KMN-167a, is very small compared to other Pleistocene European specimens of *S. hundsheimensis*. Nevertheless, the antero-posterior diameter of the proximal articular surface falls into the range of *S. hundsheimensis*. Additionally, the dimensions of the proximal articular surface of TSR-G16-41 fall into the range of *S. hundsheimensis,* and close to the smaller specimens of this species (Fig. 10).

Stephanorhinus sp.

Material. Maxilla with right and left P2–M3 (lacking left M1), TSR-G17-6; maxilla with left P3–M3, TSR-F20-24; maxilla with P3, M1, M2 (damaged DP4), KRI-16/1978; maxilla with DP3, DP4, and M1, PLN-1; mandibular corpora with right p2–p4 and left p4, TSR-D18-24; left mandibular corpora with m2–m3, VOL-223bc; DP4, TSR-G21-47, APL-498; P3, KRI-17/1978; P4, TSR-F14-19, KRI-18/1975; M2, TSR-E19-19; M3, TSR-D19-8, TSR-165, TSR-E19-10, TSR-H15-16; upper premolar, DFN-341; upper molar, RIZ-26; lower molar, TSR-G21-29, TSR-F20-14, TSR-G21-21; atlas, LIB-336, TSR-C15-11a; axis, TSR-C15-11b; third cervical vertebra (C3), TSR-C15-11c; cervical vertebras, KMN-90a, KMN-90b, KMN-90c, KMN-90d; distal epiphysis of humerus, TSR-D13-22; proximal epiphysis of ulna, TSR-E20-8, TSR-G16-16, TSR-G21-71 (articulated with TSR-G21-70); proximal epiphysis of radius, TSR-G21-70; proximal epiphysis of McIV, TSR-F18-67; diaphysis of femur, KMN-3; astragalus, KRI-23/1978, KMN-100; fragment of calcaneus, APL-665; distal epiphysis of MtII, VOL-216.

Descriptions and comparisons. Cranial and mandibular material. The two maxillae from TSR are poorly preserved. TSR-G17-6 bears the very worn right and left P2–M3 (the left M1 is missing), lacking observable diagnostic features. The specimen TSR-F20-24 is a left maxilla with P3–M3 with limited characters, strong paracone fold at P4; a double crochet at M1; a multiple (3) crochet (or a double crochet and a single crista); and a single crochet, without crista and antecrochet.

KRI-16/1978 (SI Fig. S5) is a left maxilla with P3, damaged DP4, M1 and M2. The P3 shows a strong paracone fold; a distally horizontal continuous cingulum; and a strong crochet. The DP4 is strongly damaged, with only part of the ectoloph preserved. In the M1, the ectoloph is not preserved; it is high crowned; and bears a strong single crochet, a single crista; an opened median valley; a closed postfossette; a weak protocone constriction, and a continuous and oblique distal cingulum. The M2 has a trapezoidal occlusal outline; it is high crowned, with a strong single crochet, an antecrochet, an opened median valley with a weak protocone constriction limited at the base of the cone; and an oblique, strong and continuous distal cingulum.

PLN-1 (SI Fig. S4) is a maxilla with the alveoli of DP2, the left DP3, DP4 and M1 preserved. On the right side there are no teeth preserved. The DP3 is slightly damaged, with closed medifossette and postfossete; moderately strong ectoloph; a lingual cusp; a mesial and lateral horizontal cingulum. The DP4 has moderately strong ectoloph; strong paracone fold; mesial horizontal cingulum; a lingual cusp; strong single crochet; small crista and a moderate protocone constriction; and developed parastyle with wide parastyle groove. M1 has moderate ectoloph, with strong paracone fold; strong single crochet; moderate protocone constriction and a mesial horizontal cingulum.

TSR-D18-24 (SI Fig. S6) includes two mandibular corpora preserving the left p2–p4 and the right p4. Their poor preservation prohibits the description and comparison because either the talonid or the trigonid of each tooth is damaged. The right p4 however preserves U-shaped lingual valleys whose bottoms have great height difference, and a deep and wide vestibular groove. Moreover, the left side teeth preserve deep and wide vestibular grooves and the p3 has a U- shaped posterior lingual valley.

VOL-223bc preserves the m2 and m3 which are damaged at the lingual part. Both teeth have closed (sharped angle) and deep vestibular syncline, and the posterior valley of m3 is broad V-shaped. Both preserve mesial and lingual oblique cingulum.

Remarks. The studied cranial material includes four maxillae, two from TSR (TSR-G17-6 and F20-24) which are either in very poor preservation, or/and of very old individuals (worn teeth), not allowing any morphological or biometrical comparison and thus assigned as *Stephanorhinus* sp. The presence of a mesial cingulum on the M1 of the maxilla PLN-1 (originally attributed to *S. hundsheimensis* in Konidaris et al., 2015) is considered as a distinguishing character between *S. hundsheimensis* where it is

always present and *S. jeanvireti* where it is always absent (Ballatore & Breda, 2013; Tsoukala, 2018). However, the non-metric characters of *S. hundsheimensis* and *S. etruscus* have minor differences (Fortelius et al., 1993). PLN-1 differs from *S. kirchbergensis* which has large sized teeth with smooth enamel surface (Fortelius et al., 1993) and from *S. hemitoechus* in its less hypsodont teeth (Tsoukala & Guérin, 2016). The length of the M1 from PLN-1 (maximum length = 51.9 mm) falls into the range given by Guérin (1980) for *S. etruscus* (50.5–57.5 mm) which is overlapping with that of *S. hundsheimensis* (44.5–63.5 mm); however, it is closer to the mean of the latter taxon. In any case the available features and data are inadequate and therefore we attribute PLN-1 to *Stephanorhinus* sp.

The left maxilla from KRI (KRI-16/1978) shows similarities with *S. hundsheimensis* form Voigstedt (Kahlke, 1965; Germany, IQW 1966/7415), such as the open median valleys in the M1, M2 and P3. Considering the similar wear of the teeth, they also share the single crochet, and the single antecrochet in the M2, plus the presence of a single crochet in the M1. On the contrary, the molars of the specimen KRI-16/1978 differ from *S. hundsheimensis* in the less developed lingual cingulum (which is always present in the M1 and M2 of *S. hundsheimensis* according to Ballatore & Breda, 2013).

There are two studied mandibles, one from TSR (TSR-D18-24) and one from VOL (VOL-223bc), which do not preserve enough diagnostic features, limiting their attribution to *Stephanorhinus* sp.

Isolated teeth. TSR-G21-47 (SI Fig. S6) and APL-498 (isolated DP4) preserve a strong single crochet, weak protocone constriction, and a strong paracone fold. TSR-G21-47 has no crista, and the mesial continuous cingulum is horizontal. On the contrary APL-498 shows an oblique mesial cingulum and a single crista with a tiny cusp.

KRI-17/1978 (SI Fig. S5), is a right high crowned P3 with very high ectoloph, damaged at the mesial part. The mesial cingulum is strong, horizontal, and continuous and the lingual cingulum is oblique, and continuous.

TSR-F14-19 (SI Fig. S6) is a right P4 with a single crochet and a crista, quite worn with closed median valley and remnants of a mesial cingulum.

KRI-18/1975 (SI Fig. S5) is a right high crowned P4 that shows a strong paracone fold; a moderately developed parastyle and metastyle; a closed postfossette; a double crochet; a single crista; a horizontal and continuous mesial cingulum and closed median valley.

TSR-E19-19 is a poorly preserved left M2 with a single crochet and a single crista.

All the TSR M3 preserve a double crochet; TSR-D19-8 and TSR-E19-10 (SI Fig. S6) have a broad and strong paracone fold; TSR-D19-8 and TSR-H15-16 preserve a single crochet. TSR-165 is a very fragmented M3 with a possible single crochet.

DFN-341 is a very worn-out upper premolar, probably P2. RIZ-26 is a worn upper left premolar with a single crochet and a small crista. The ectoloph is almost straight and no cingula are present or preserved.

TSR-G21-29 (SI Fig. S6) is a right lower molar with an acute angle of vestibular groove; a small vestibular cingulum occurs at the talonid while the trigonid is partially preserved. TSR-F20-14 is a fragment of a left lower tooth and based on the size probably a molar. The specimen TSR-G21-21 is a tooth fragment from the right side with a shallow vestibular groove.

Remarks. Deciduous and isolated teeth are not diagnostic at species level, therefore the specimens TSR-G21-47, APL-498, KRI-1978, TSR-F14-19, KRI-18-1975, TSR-E19-19, TSR-D19-8, TSR-65, TSR-E19-10, TSRH15-16, DFN-341, RIZ-26, TSR-G21-29, TSR-F20-14, TSR-G21-21 are referred to as *Stephanorhinus* sp.

Vertebrae. The two atlases, TSR-C15-11a and LIB-336 (SI Fig. S1), show in dorsal view a strongly marked dorsal tubercle; a shallow U-shaped superior notch in ventral view; wide and round articular surfaces for the occipital condyles in anterior view; and narrow and transversally elongated posterior articular surfaces for the axis in posterior view.

The dorsal arch of the axis TSR-C15-11b is more robust in dorsal view, and the anterior articular surfaces are transversally elongated.

TSR-C15-11c is a very damaged third cervical vertebra in poor state, preserving only remains of the left transverse foramen and part of its transversal arc. The neural spine of the cervical vertebrae KMN-90a, KMN-90b, KMN-90c have a moderate height, except for KMN-90d, where it is partially preserved, their transverse foramen is wide, with limited height.

Remarks. The literature that is currently available for comparing vertebrae of the genus *Stephanorhinus* is extremely limited to the following sources: Guérin (1972) who provided measurements of the atlas of *S. jeanvireti* from Vialette (France) compared to *Pliorhinus megarhinus* and *S. etruscus;* Tsoukala and Guérin (2016) who described vertebrae of *S. hemitoechus* from Petralona (Greece); and Fortelius et al (1993), where there is only some measurements and no morphological comparison. Furthermore, there are descriptions of juvenile *Coelodonta nihowanensis* from China (Tong & Wang, 2014), and *Coelodonta antiquitatis* from France (Guérin, 1973). As a result, the vertebrae LIB-336, TSR-C15-11a, TSR-C15-11b, TSR-C15-11c, KMN-90a-d are attributed to *Stephanorhinus* sp.

Humerus. The badly preserved TSR-D13-22 is a transversally elongated left humerus. The medial lip of the trochlea is curved and slightly concave. The axis of the trochlea is oblique, and the groove is deep and wide. In posterior view, the olecranon fossa has greater width than height.

Remarks. TSR-D13-22 is more robust proportionally than the *S. etruscus* TSR-133, but too fragmented for a certain assignment.

Radius and ulna. The ulnae TSR-G16-16, TSR-E20-8 and TSR-G21-71 have the proximal epiphysis and part of their diaphysis preserved, without the olecranon. The trochlea notch is asymmetric. The difference in height of the distal edge of the medial lip from the lateral articular surface is small, apart from TSR-G21-71 where it is great. The lateral border of the lateral articular surface is parallel to the corpus of the bone, apart from TSR-G16-16. In lateral view, a shallow and narrow or blunt groove delimits the trochlea notch, whereas the walls of the diaphysis are flat except for the medial and the lateral ones which are slightly concave.

In proximal view the medial articular surface of the radius TSR-G21-70 is damaged at the medial and anterior part. The lateral articular surface is concave and square with rounded edges; its posterior border is straight and oblique, forming a 45° angle. The posterior border of the entire articulation forms an obtuse angle, ~ 120°. In anterior view, both radial and lateral tuberosities are evident. In anterior view, the proximo-lateral border is concave whilst the lateral is almost straight.

Remarks. The diagnostic characteristics of ulnae between Pleistocene European *Stephanorhinus* species are quite limited. Several research mentioned some characters (e.g., Lacombat, 2005; Stefanelli et al., 2024) focusing on the breadth of the olecranon or the prominence of the anconeus process, characters that appear however variant, not allowing a taxonomy at species level. Therefore, the ulnae specimens TSR-E20-9, TSR-G16-16, TSR-G21-71 are ascribed to *Stephanorhinus* sp.

The radius TSR-G21-71 is too fragmented for comparison and does not preserve diagnostic features, hence it is attributed to *Stephanorhinus* sp.

Metacarpals. In proximal view, the proximal articular surface of McIV TSR-F18-67 has the shape of an equilateral triangle with rounded corners. The anterior border in proximal view is slightly wavy but strongly concave in anterior view. In proximal view, the medial border is convex, and the latero-posterior one is straight with a concavity posteriorly to the articular surface for the McIV, which is in contact with the proximal articular surface and almost circular. In medial view, there are two articular surfaces for the McIII and the magnum, clearly distinct from each other. The anterior one is elongated triangular shaped and in contact with the proximal articular surface. The posterior one is elongated vertically and elliptical shaped. The cross-section of the preserved diaphysis close to the proximal epiphysis is triangularly shaped.

Remarks. Diagnostic characters for the McIV for the different species are very limited, especially those that distinguish *S. hundsheimensis* from *S. etruscus*. Stefanelli et al. (2024) mention a total of four characters, of which the three are similar in both *S. hundsheimensis* and *S. etruscus.* The only character different in these two species is the anterior border of the proximal epiphysis, which is described as 'highly concave' in *S. etruscus* and 'concave' in *S. hundsheimensis* (Lacombat, 2005; Stefanelli et al., 2024). The anterior border of the proximal epiphysis of TSR-F18-67 is as concave as in CM 30703 of *S. hundsheimensis* from Contrada Monticelli, whose preservation though is fragmentary (Stefanelli et al., 2024). Until there is more adequate comparative material, we prefer an attribution to *Stephanorhinus* sp.

The absolute dimensions of the proximal epiphyses of the McIV of Pleistocene rhinoceroses show that *S. etruscus* is the smaller, followed by *S. hemitoechus* and *S. hundsheimensis* and progressively by *S. jeanvireti*. *Stephanorhinus etruscus* and *S. hemitoechus* have similar ranges of antero-posterior diameter, however *S. hemitoechus* has greater transversal diameter. *Stephanorhinus jeanvireti* has greater PTD values with a transversal diameter similar to the one specimen of *S. kirchbergensis*. TSR-F18-67 is larger than *S. etruscus*, however it is in the middle of the range of *S. hemitoechus* and *S. hundsheimensis* and close to the smaller values of *S. jeanvireti* (Fig. 14).

Femur: The specimen KMN-3 is a right sub-adult femur with the unfused distal epiphysis missing. The proximal epiphysis has only the rounded and slightly projecting femoral head preserved.

Remarks. The femoral diaphysis KMN-3 belongs to a sub-adult individual (the distal epiphysis is not completely fused). Its dimensions are close to those of the specimen TSR-F8-81 and the smaller values of *S. hundsheimensis* (Fig. 13).

Astragalus. The trochlea of both astragali, KRI-23/1978 and KMN-100, have a weak inclination and deep trochlea groove, though that of KMN-100 has a transversally elongated medial lip in anterior view. The depression distally the trochlea is reduced in KRI-23/1978 but deep and high in KMN-100. In medial view, the medial tuberosity of KRI-23/1978 is rounded, well-marked and disto-posteriorly located, while in KMN-100 is distally located. In distal view, the medial articular surface of KRI-23/1978 is

rhomboidal-shaped, with a smooth crest separating from the lateral one. In the same view, the medial articular surface of KMN-100 is rectangular, the lateral one is orthogonal and the crest separating them is acute anteriorly but smooth towards the posterior side.

Remarks: The morphology of KRI-23/1978, APL-213 and KMN-100 is very similar in anterior view. However, the astragalus KMN-100 has a certain pathology and for this reason, any morphological comparison should be considered with caution. The preservation of KRI-23/1978 is too bad to identify it at the species level, therefore it is referred to as *Stephanorhinus* sp.

Calcaneus. APL-665 is a fragment of a calcaneus lacking diagnostic features. Only part of the *sustentaculum talii* is preserved, which is not enough to identify it at the species level.

MtII. VOL-216 is a distal epiphysis of MtII with part of the diaphysis and with narrow and asymmetrical distal trochlea. The fragmentary nature of the specimen does not allow for a specific attribution.

Discussion

Based on the most recent review of Rhinocerotidae in Greece (Giaourtsakis, 2022), the Pleistocene fossil rhino record is very scarce (Fig. 15), and as a result most of the specimens are classified as "Rhinocerotidae indet". In the present study, the re-examination of the older collected material and the study of new one aims to improve the taxonomy and shed light on the biochronology of the rhinoceroses of Greece. The rhinoceros taxa recovered from the fossiliferous localities included in this study are summarized in the Table 1.

Stephanorhinus jeanvireti is a much larger-sized, but still slender, rhino, with a massive facial area and long and broad nasal bones; its diet was browse-dominated (Lacombat, 2007). It lived in humid, forest-dominated environments with relatively open areas, where Gramineae and ferns grew (Guérin, 1980; Lacombat & Mörs, 2008; Szabó et al., 2017; Tsoukala, 2018). It is mainly present in MN 16, however it survived until the Early Pleistocene in Romania (MNQ18; Pandolfi et al., 2019). In Greece, *S. jeanvireti* is known so far only from three localities, Milia, Angelochori and Saint George Priporos, all dated to the Late Pliocene, MN16 (Guérin & Tsoukala, 2013; Tsoukala, 2018; Giaourtsakis, 2022). The presence of *S.* cf. *S. jeanvireti* at DFN3 marks its last known occurrence in Greece, in agreement with the Colțești record (Romania; Pandolfi et al., 2019). Furthermore, considering the DFN record, which is roughly isochronous with those from Vatera DS and VOL, it seems that *S. etruscus*

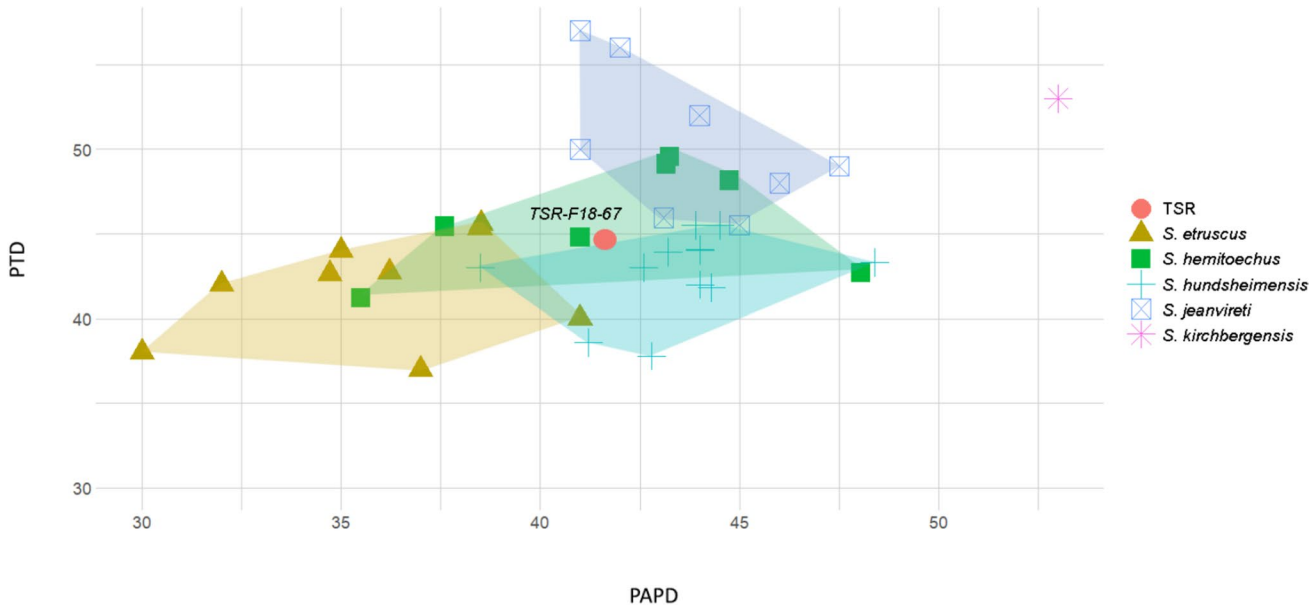

Fig. 14 Scatter plot of the proximal transversal diameter (PTD) and the proximal antero-posterior diameter (PAPD) the McIV TSR-F18-67, in mm. Comparative material from: Guérin and Heintz (1971); Guérin (1972); Cerdeño (1990); Mazza et al., (1993); Fortelius et al. (1993); Kahlke (2001); Lacombat (2005); Pandolfi and Tagliacozzo (2015); Pandolfi et al. (2017); García-Fernández et al. (2023); Stefanelli et al. (2024)

co-occurred for a short time period with *S. jeanvireti* during the Early Pleistocene in Greece (Fig. 16).

Stephanorhinus etruscus and *S. jeanvireti* first occurred in MN16a throughout Europe (Cirilli et al., 2020). The first one is a slender, small-sized cursorial rhino, with head posture suggesting a primarily browsing diet, low crowned teeth, and shallow joints, suggesting locomotion in open woodlands (Loose, 1975; Fortelius et al., 1993). It is one of the most abundant and widespread *Stephanorhinus* species in Europe, including Greece. Its earliest European occurrences are from uppermost Pliocene Spanish, Italian, French and Romanian localities (Pandolfi et al., 2017 and references therein). Its last occurrences are debatable, and likely diachronic in different Eurasian areas. In Greece *S. etruscus* (Aivaliki, Richea, Libakos, Kalamoto 1, 2) or *S.* cf. *etruscus* (Psychiko, Molikrio, Vatera DS, Aivaliki, Tourkovounia 3–5) is reported from various localities spanning from the middle Villafranchian (MNQ17) to the late Villafranchian (Giaourtsakis, 2022, and references therein).In this study we confirmed the presence of *S. etruscus* in VOL, LIB, TSR and APL. The presence of *S. etruscus* at VOL likely marks its first confirmed Greek record and roughly coincides chronologically with that of Vatera DS in Lesvos Island. Late Villafranchian *S. etruscus* was already known in Greece from LIB, and it is further supported here by the TSR record at ca 1.7 Ma. The last occurrence of *S. etruscus* in Greece is marked at APL, dated close to late Villafranchian/Epivillafranchian boundary, at ca. 1.2 Ma. In conclusion, *S. etruscus* is present in Greece from ca. 2.4–2.3 Ma to ca. 1.2 Ma. Although the species seems to disappear from Central Europe slightly earlier (Pandolfi et al., 2017) it persists until 1.2–1.0 Ma in Italy, Iberian Peninsula and according to our data also in Greece.

Stephanorhinus hundsheimensis is commonly misidentified with other taxa. It is a long-legged rhino that lived in open woodland xeric grassland (Szabó et al., 2017) with a head posture suggesting a mixed diet of both grazing and browsing. According to some authors this dietary variability might have been the reason for its extinction, as this species was replaced by more specialized browsers (*S. kirchbergensis*) or grazers (*S. hemitoechus*) (Kahlke & Kaiser, 2011). *Stephanorhinus hundsheimensis* is reported from Europe and Turkey since the late Early Pleistocene (ca. 1.2 Ma) (Pandolfi & Erten, 2017). It is present in several localities in central Europe (France, Germany), in the Italian and Iberian Peninsulas, as well as in Romania (Pandolfi & Erten, 2017; and references therein). The lineage *Stephanorhinus* ex gr. *etruscus/hundsheimensis* has been recorded in Dmanisi (Georgia) establishing its first occurrence (Pandolfi et al., 2021b). Its last occurrence is documented in Cova del Rinoceront, dated to ca. 175–74 ka (García-Fernández et al., 2023).

In Greece, *S. hundsheimensis* was documented as the earliest evidence of large animal fossil collecting in mainland Greece, as reported from an astragalus studied at Bronze Age Mycenae (Meier et al., 2024). Except from this specimen, it was reported from PLN (Konidaris et al., 2015), based on a maxilla fragment with deciduous teeth that is here, however, assigned to *Stephanorhinus* sp., in agreement with Giaourtsakis (2022). It was also reported from APL (Konidaris et al., 2015), nevertheless the revision of APL material shows that it is morphologically and dimensionally closer to *S. etruscus*. On the contrary, material from KRI previously attributed to *S. etruscus* (Sakellariou et al., 1979) is here recognized as *S.* cf. *S hundsheimensis.* The presence of *S. hundsheimensis* at RIZ, KRI and KMN and TSR, likely represent the first and earliest record of this species in Greece. The age of RIZ (possibly ca. 1.2 Ma) coincides with the appearance of the species in both Europe (Vallparadís in Spain, Vallonet in France, Untermassfeld in Germany; Guérin, 1980; Kahlke, 2001, 2022; Lacombat & Moullé, 2005; Madurell-Malapeira et al., 2010) and Anatolia (Denizli, Pandolfi & Erten, 2017). The possible presence of *S. hundsheimensis* at KRI, KMN and especially at TSR, where it co-occurs with *S. etruscus*, indicates that the species may have entered earlier into SE Europe at least, at ca. 1.7 Ma. It is worth mentioning that the co-occurrence of *S. etruscus* and *S.* cf. *S. hundsheimensis* in the same locality is confirmed for the first time, as they are generally thought to occupy different habitats (Pandolfi et al., 2021b). Another hypothesis could be the presence of the two rhinoceros' species with different diets sharing the same habitat. *S. hundsheimensis* considered the most ecologically flexible rhinoceros, exhibits a diet that varies from predominantly browsing to predominantly grazing, indicative of mixed feeding habits (Kahlke & Kaiser, 2011). Conversely, *S. etruscus* is characterized by browsing habits, as evidenced by both mesowear and microwear analyses (Rivals & Lister, 2016). Their coexistence has been reported in Trlica (Montenegro), however from different stratigraphic layers and based on isolated teeth (Vislobokova & Agadjanian, 2015); this led Pandolfi et al. (2017) to question their common presence. The relationships between *S. hundsheimensis* and other *Stephanorhinus* species is still debated. Guérin (1980) suggests the evolution of both *S. hundsheimensis* (= *Dicerorhinus etruscus brachycephalus* in partim in Guérin, 1980) and *S. hemitoechus* from *S. etruscus*, whereas others link *S. hundsheimensis* with *S. jeanvireti* (Fortelius et al., 1993; Lacombat, 2007) or to a taxon that migrated from Asia (Mazza, 1988). In Pandolfi (2023), *S. jeanvireti* resulted as the early divergent *Stephanorhinus* species, with *S. etruscus* as sister taxon of *S. hundsheimensis*, *S. kirchbergensis* and *S. hemitoechus* clade.

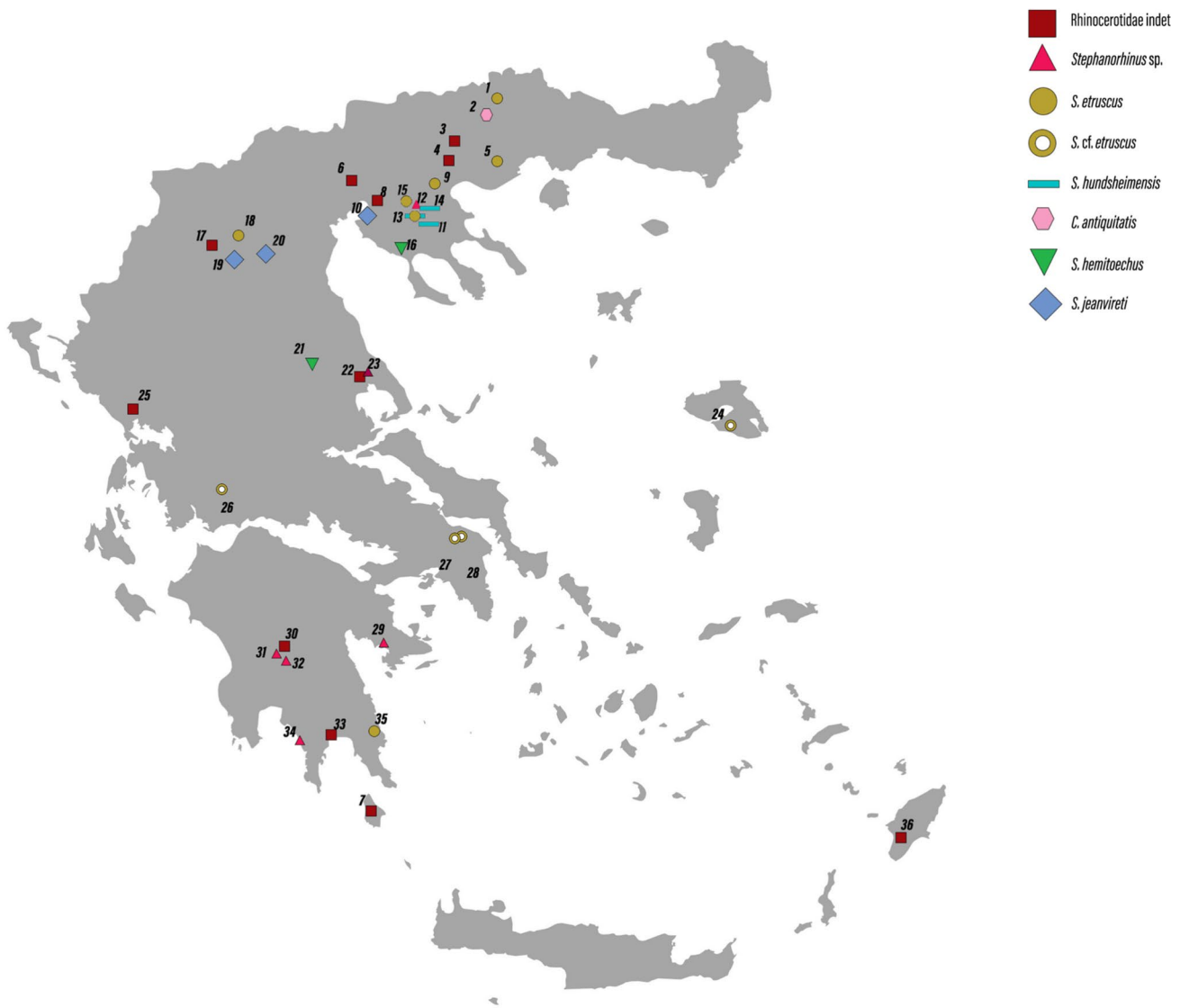

Fig. 15 Pleistocene localities of Greece wth rhinocerotids (updated from Giaourtsakis, 2022), including the revised material from this study. 1, Volax; 2, Aggitis; 3, Serres Basin; 4, Nigrita; 5, Aivaliki; 6, Gephyra; 7, Kythera; 8, Agia Triada; 9, Apollonia-1; 10, Angelochori; 11, Riza-1; 12, Platanochori-1; 13, Tsiotra Vryssi; 14, Krimni-1, 3; 15, Kalamoto-1, 2; 16, Petralona; 17, Neapolis; 18, Libakos; 19, Milia; 20, Dafnero-3; 21, Penios riverbank; 22, Alikes; 23, localities of Sesklo; 24, Vatera; 25, Asprochaliko; 26, Molikrio; 27, Tourkovounia 3-5; 28, Psychiko; 29, Karnezeika; 30, Marathousa Member (Megalopolis Basin, "Sickenberg's material"); 31, localities of Megalopolis Basin ("Skouphos'/Meletis' material"); 32, Kyparissia mine and Kyparissia 4, Megalopolis Basin; 33, Lakonis-1; 34, Kalamakia; 35, Richea; 36, Apolakkia. Source: Vemaps.com, modified

Conclusions

The limited and usually fragmentary rhinocerotid material in most Pleistocene localities studied here make their systematic attribution challenging. Nevertheless, based on morphological and morphometric comparison, we reviewed or re-ascribed several taxa from several Pleistocene sites of Greece. *Stephanorhinus* cf. *S. jeanvireti* from Dafnero

Table 1 Age of the localities included in the study (based on selected references and updates in Konidaris & Kostopoulos, 2024) and taxonomy of the rhinoceroses

Locality	Literature	Age	Attribution
Dafnero-3	Benammi et al. (2020)	~2.3 Ma	*S.* cf. *S. jeanvireti*
Volax	Koufos and Vlachou (1997)	2.5 to 2.0 Ma	*S. etruscus*
Tsiotra Vryssi	Konidaris et al., (2015, 2021)	1.78 to ~1.6 Ma	*S. etruscus* *S.* cf. *S. hundsheimensis*
Libakos	Koufos (2001)	1.6 to 1.5 Ma	*S. etruscus*
Krimni-1, 3	Sakellariou et al. (1979); Kostopoulos et al. (2023)	1.6 to 1.5 Ma	*S.* cf. *S. hundsheimensis*
Platanochori-1	Konidaris et al. (2015)	?1.2 Ma	*Stephanorhinus* sp.
Riza-1	Koufos (2001)	?1.2 Ma	*S.* cf. *S. hundsheimensis*
Apollonia-1	Koufos et al. (1995)	ca. 1.2 Ma	*S. etruscus*

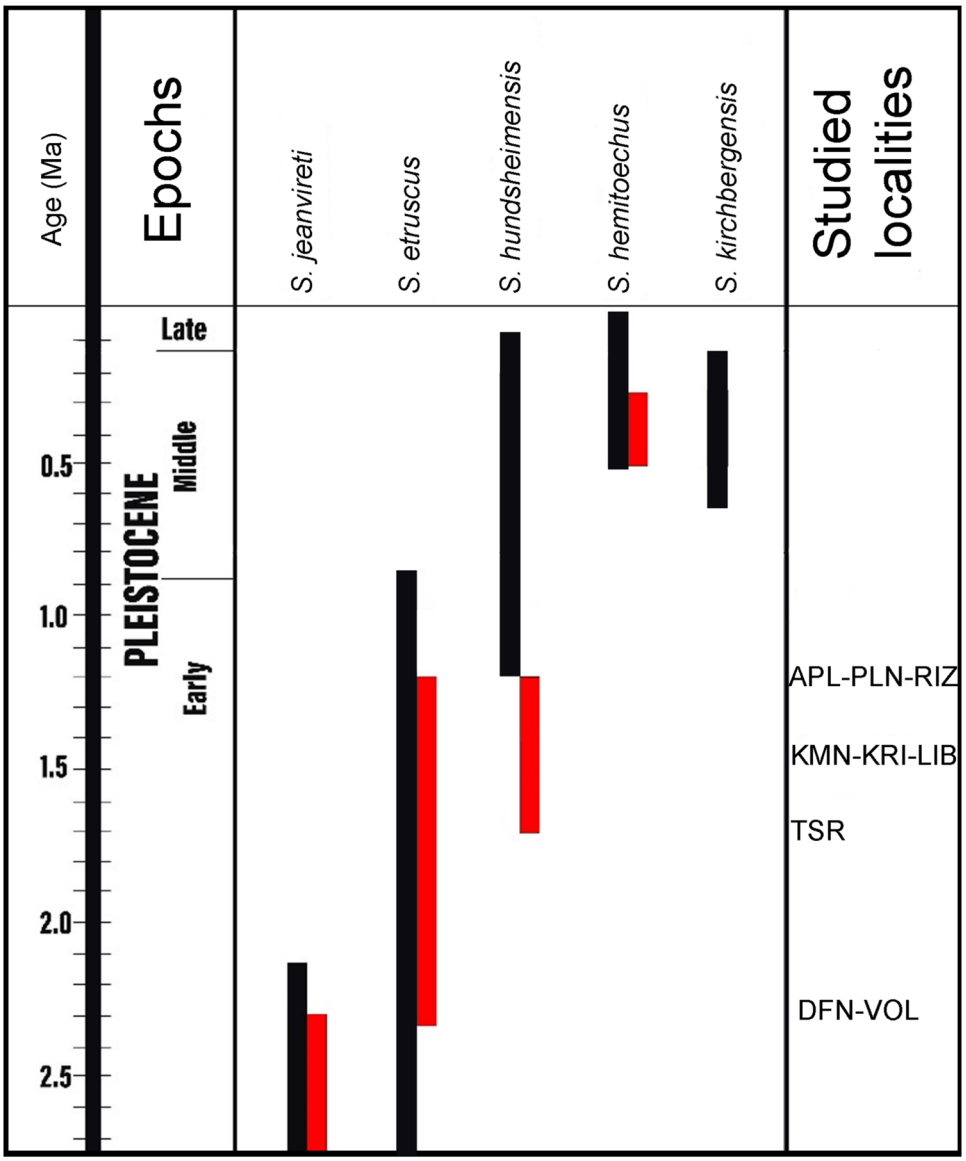

Fig. 16 Biochronological range of Pleistocene Rhinocerotidae in Europe (black) and Greece (red). Data from: Masini and Sala (2007); Agustí et al. (2009); Pandolfi et al. (2018); Puzachenko et al. (2021); García-Fernández et al. (2023)

corresponds to the last so far known occurrence of this species in Greece, also establishing a short time of coexistence with *S. etruscus*, already known from Tourkovounia (3–5) and Volax. *Stephanorhinus etruscus* is similarly confirmed in Libakos and Apollonia-1, altogether spanning in Greece from 2.3 to ~ 1.2 Ma. *Stephanorhinus* cf. *S. hundsheimensis* is also confirmed at Krimni-1, 3, Tsiotra Vryssi and Riza-1, establishing the possible presence of this species in Greece from ca. 1.78 to possibly 1.2 Ma. The record of Tsiotra Vryssi in particular suggests that *S. hundsheimensis* possibly appeared earlier in SE Europe and confirms its co-existence there with *S. etruscus*.

Supplementary Information The online version contains supplementary material available at https://doi.org/10.1007/s12542-025-00739-8.

Acknowledgements Excavation at TSR was supported by the ERC Consolidator Grant ERC-CoG-724703 ('CROSSROADS') and the ERC Starting Grant ERC-StG-283503 ('PaGE'), both awarded to K. Harvati. G.K. was supported by the Deutsche Forschungsgemeinschaft (DFG Project no. 463225251, "MEGALOPOLIS"). K.C. thanks the curators of IGF-NHMF, Geological and Paleontological Section of the Natural History Museum of Florence, Italy. We thank P.A. Tleuberdina and one anonymous reviewer for the constructive comments and suggestions that improved the manuscript.

Author contributions Conceptualization D.S.K, G.K.; validation, D.S.K., G.K., L.P., K.C.; formal analysis, K.C.; data curation, K.C.; writing-original draft preparation, K.C.; writing review and editing, K.C., G.K., L.P., D.S.K; Visualization, K.C.; All authors have read and agreed to the published version of the manuscript.

Funding Open Access funding enabled and organized by Projekt DEAL. Excavation at TSR was supported by the ERC Consolidator Grant ERC-CoG-724703 ('CROSSROADS') and the ERC Starting Grant ERC-StG-283503 ('PaGE'), both awarded to K. Harvati. G.K. was supported by the Deutsche Forschungsgemeinschaft (DFG Project no. 463225251, "MEGALOPOLIS"). K.C. is supported by the ERC-AdG-101019659("FIRSTSTEPS").

Data availability statement All data analysed during this study are included in this published article. All fossil material described in this paper is deposited in a Public Institution (Museum of Geology-Palaeontology-Palaeoanthropology, Aristotle University of Thessaloniki) and is freely accessible to any researcher upon request.

Declarations

Conflict of interest The authors have no competing interests to declare that are relevant to the content of this article nor have financial or proprietary interests in any material discussed in this article.

References

Agustí, J., Vekua, A., Oms, O., Lordkipanidze, D., Bukhsianidze, M., Kiladze, G., & Rook, L. (2009). The Pliocene-Pleistocene succession of Kvabebi (Georgia) and the background to the early human occupation of Southern Caucasus. *Quaternary Science Reviews, 28*, 3275–3280.

Ballatore, M., & Breda, M. (2013). *Stephanorhinus hundsheimensis* (Rhinocerontidae, Mammalia) teeth from the early Middle Pleistocene of Isernia La Pineta (Molise, Italy) and comparison with coeval British material. *Quaternary International, 302*, 169–183. https://doi.org/10.1016/j.quaint.2013.02.002

Benammi, M., Aidona, E., Merceron, G., Koufos, G. D., & Kostopoulos, D. S. (2020). Magnetostratigraphy and chronology of the Lower Pleistocene primate bearing Dafnero fossil site, N. Greece. *Quaternary, 3*, 22. https://doi.org/10.3390/quat3030022

Caloi, L., & Palombo, M. R. (1978). Anfibi, rettili e mammiferi di Torre del Pagliaccetto (Torre in Pietra, Roma). *Quaternaria, 20*, 315–428.

Cerdeño, E. (1990). *Stephanorhinus hemitoechus* (Falc.) (Rhinocerotidae, Mammalia) del Pleistoceno medio y superior de España. *Estudios Geológicos, 479*, 465–479. https://doi.org/10.3989/egeol.90465-6475

Chitoglou, K., Pandolfi, L., & Kostopoulos, D. S. (2023). First occurrence of *Pliorhinus* cf. *megarhinus* (Perrissodactyla, Rhinocerotidae) in Greece. *Bulletin of the Geological Society of Greece, 60*(1), 1–13. https://doi.org/10.12681/bgsg.33711

Cirilli, O., Pandolfi, L., & Bernor, R. L. (2020). The Villafranchian perissodactyls of Italy: Knowledge of the fossil record and future research perspectives. *Geobios, 63*, 1–21. https://doi.org/10.1016/j.geobios.2020.09.001

Fortelius, M., Mazza, P., & Sala, B. (1993). *Stephanorhinus* (Mammalia: Rhinocerotidae) of western European Pleistocene, with a revision of *S. etruscus* (Falconer, 1868). *Palaeontographia Italica, 80*, 63–155.

García-Fernández, D., Cerdeño, E., Sanz, M., & Daura, J. (2023). The latest occurenceof *Stephanorhinus hundsheimensis* (Rhinocerotidae) in Europe: The skeletonsfrom the Cova del Rinoceront site (Castelldefels, Barcelona). *Quaternary, 6*(4), 60. https://doi.org/10.3390/quat6040060

Giaourtsakis, I. X. (2022). The fossil record of rhinocerotids (Mammalia: Perissodactyla: Rhinocerotidae) in Greece. In *Fossil vertebrates of Greece Vol. 2: Laurasiatherians, artiodactyles, perissodactyles, carnivorans, and island endemics* (pp. 409–500). https://doi.org/10.1007/978-3-030-68442-6_14

Gibbard, P. L., Head, M. J., Walker, M. J., The Subcommission on Quaternary Stratigraphy. (2010). Formal ratification of the Quaternary system/period and the Pleistocene Series/Epoch with a base at 2.58 Ma. *Journal of Quaternary Science, 25*(2), 96–102.

Guérin, C. (1972). Une nouvelle espèce de rhinocéros (Mammalia, Perissodactyla) à Vialette (Haute-Loire, France) et dans d'autres gisements du Villafranchien inférieur européen: *Dicerorhinus jeanvireti* n. sp. *Documents des Laboratoires De Géologie De La Faculté des Sciences De Lyon, 49*, 53–150.

Guérin, C. (1973). Les trois espèces de rhinocéros (Mammalia, Perissodactyla) du gisement Pleistocene moyen des Abîmes de la Fage à Noailles (Corrèze). *Publications Du Musée des Confluences, 11*(1), 55–84. https://doi.org/10.3406/mhnly.1973.1010

Guérin, C. (1980). Les rhinoceros (Mammalia, Perissodactyla) du Miocene terminal au Pleistocene superieur en Europe occidentale: Comparison avec les especes actuelles. *Documents des Laboratoires de Géologie de Lyon, 79*, 1–1185.

Guérin, C. (2004). Les rhinocéros (Mammalia, Perissodactyla) du gisement villafranchien moyen de Saint-Vallier (Drôme). *Geobios, 37*, 259–278.

Guérin, C., & Heintz, E. (1971). *Dicerorhinus etruscus* (Falconer, 1859), Rhinocerotidae, Mammalia, du Villafranchien de la Puebla de Valverde (Teruel, Espagne). *Bulletin du Museum National d'Histoire Naturelle., 3*(18), 13–22.

Guérin, C., & Tsoukala, E. (2013). The Tapiridae, Rhinocerotidae and Suidae (Mammalia) of the Early Villafranchian site of Milia (Grevena, Macedonia, Greece). *Geodiversitas, 35*, 447–489. https://doi.org/10.5252/g2013n2a7

Iurino, D. A., Conti, J., Mecozzi, B., & Sardella, R. (2020). Braincase with natural endocast of a juvenile Rhinocerotinae from the Late Middle Pleistocene site of Melpignano (Apulia, Southern Italy). *Frontiers in Earth Science, 8*, 1–14. https://doi.org/10.3389/feart.2020.00094

Kahlke, H.-D. (1975). Die Rhinocerotiden-Reste aus den Travertinen von Weimar-Ehringsdorf. In H.-D. Kahlke (Ed.), *Das Pleistozän von Weimar-Ehringsdorf* (pp. 337–397).

Kahlke, H.-D. (2001). Die Rhinocerotiden-Reste aus dem Unterpleistozän von Untermaßfeld. In *Das Pleistozän von Untermaßfeld Bei Meiningen (Thüringen),* Teil 2 (pp. 501–555).

Kahlke, R. D. (2022). The Pleistocene of Untermaßfeld—A synopsis of site origin, palaeobiodiversity, taphonomic characteristics, palaeoenvironment, chronostratigraphy, and significance in western Palaearctic faunal history. In R. D. Kahlke (Ed.), The Pleistocene of Untermaßfeld near Meiningen (Thüringen, Germany). Part 5. *Monographien des Römisch-Germanischen Zentralmuseums Mainz, Mainz* (pp. 1635–1734).

Kahlke, H. D. (1965). The rhinocerotid remains from the clays of Voigtstedt in Thuringia. *The Pleistocene of Voigtstedt, Paleontological Treatises, A, II*(2/3), 451–519.

Kahlke, R. D., & Kaiser, T. M. (2011). Generalism as a subsistence strategy: Advantages and limitations of the highly flexible feeding traits of Pleistocene *Stephanorhinus hundsheimensis* (Rhinocerotidae, Mammalia). *Quaternary Science Reviews, 30*, 2250–2261. https://doi.org/10.1016/j.quascirev.2009.12.012

Konidaris, G. E., & Kostopoulos, D. S. (2024). The Late Pliocene–Middle Pleistocene large mammal faunal units of Greece. *Quaternary, 7*, 27. https://doi.org/10.3390/quat7020027

Konidaris, G. E., Kostopoulos, D. S., Maron, M., Schaller, M., Ehlers, T. A., Aidona, E., Marini, M., Tourloukis, V., Muttoni, G., Koufos, G. D., & Harvati, K. (2021). Dating of the Lower Pleistocene vertebrate site of Tsiotra Vryssi (Mygdonia Basin, Greece): Biochronology, magnetostratigraphy, and cosmogenic radionuclides. *Quaternary, 4*, 1. https://doi.org/10.3390/quat4010001

Konidaris, G. E., Kostopoulos, D. S., Maron, M., Schaller, M., Ehlers, T. A., Aidona, E., Marini, M., Tourloukis, V., Muttoni, G., Koufos, G. D., & Harvati, K. (2022). Correction: Konidaris et al. Dating of the Lower Pleistocene vertebrate site of Tsiotra Vryssi (Mygdonia Basin, Greece): Biochronology, magnetostratigraphy, and cosmogenic radionuclides. Quaternary 2021, 4, 1. *Quaternary, 5*, 21. https://doi.org/10.3390/quat5020021

Konidaris, G. E., Tourloukis, V., Kostopoulos, D. S., Thompson, N., Giusti, D., Michailidis, D., Koufos, G. D., & Harvati, K. (2015). Two new vertebrate localities from the Early Pleistocene of Mygdonia Basin (Macedonia, Greece): Preliminary results. *Comptes Rendus – Palevol, 14*(5), 353–362. https://doi.org/10.1016/j.crpv.2015.05.004

Kostopoulos, D. S. (1996). The Plio-Pleistocene artiodactyls of Macedonia (N. Greece). Systematics, palaeoecology, biochronology, biostratigraphy. Ph.D. thesis, Department of Geology, University of Thessaloniki (p. 612) (unpublished) **(in Greek)**.

Kostopoulos, D. S., Aidona, E., Benammi, M., Gkeme, A., Grasset, L., Guy, F., & Merceron, G. (2019). The Lower Pleistocene primate-bearing fossil site of Dafnero (W. Macedonia, Greece): New data from classic and innovative approaches. In *Proceedings of 15th international congress of the Geological Society of Greece*.

Kostopoulos, D. S., Konidaris, G. E., Amanatidou, M., Chitoglou, K., Fragkioudakis, E., Gerakakis, N., Giannakou, V., Gkeme, A., Kalaitzi, C., Tsakalidis, C., & Tsatsalis, V. (2023). The new fossil site Krimni-3 in Mygdonia Basin and the first evidence of a giant ostrich in the Early Pleistocene of Greece. *PalZ, 97*, 147–161. https://doi.org/10.1007/s12542-022-00632-8

Koufos, G. D. (2001). The Villafranchian mammalian faunas and biochronology of Greece. *Bollettino della Societa Paleontologica Italiana, 40*, 217–223.

Koufos, G. D., Syrides, G. E., Kostopoulos, D. S., & Koliadimou, K. K. (1995). Preliminary results about the stratigraphy and the palaeoenvironment of Mygdonia Basin, Macedonia, Greece. *Geobios, M.S. 18*, 243–249.

Koufos, G. D., & Tamvakis, A. (2022). Revising the Villafranchian carnivoran fauna from Libakos (Macedonia, Greece) with some implications for its age. *Historical Biology, 34*, 1399–1412. https://doi.org/10.1080/08912963.2021.2024179

Koufos, G. D., & Vlachou, T. D. (1997). *Equus stenonis* from the middle Villafranchian locality of Volax (Macedonia, Greece). *Geodiversitas, 19*, 641–657.

Lacombat, F. (2005). Les rhinocéros fossiles des sites préhistoriques de l'Europe méditerranéenne et du Massif Central: Paléontologie et implications biochronologiques. *British Archaeological Reports, 1419*, 1–175. https://doi.org/10.30861/9781841718583

Lacombat, F. (2006). Morphological and biometrical differentiation of the teeth from Pleistocene species of *Stephanorhinus* (Mammalia, Perissodactyla, Rhinocerotidae) in Mediterranean Europe and the Massif Central, France. *Palaeontographica Abt. A, 274*, 71–111. https://doi.org/10.1127/pala/274/2006/71

Lacombat, F. (2007). Phylogeny of the genus *Stephanorhinus* in the Plio-Pleistocene of Europe. *Hallesches Jahrb. Geowiss, 23*, 63–64.

Lacombat, F., & Mörs, T. (2008). The northernmost occurrence of the rare Late Pliocene rhinoceros *Stephanorhinus jeanvireti* (Mammalia, Perissodactyla). *Neues Jahrbuch fur Geologie und Palaontologie - Abhandlungen, 249*(2), 157–165. https://doi.org/10.1127/0077-7749/2008/0249-0157

Lacombat, F., & Moullé, P.-E. (2005). Description paléontologique du *Stephanorhinus hundsheimensis* (Toula, 1902) Pléistocène Inférieur de la Tour de Grimaldi (Liguri, Italie). *Bulletin du Museéum d'Anthropologie Préhistorique de Monaco, 44*, 33–38.

Lobachev, Y. V., Shpansky, V., Bondarev, A. A., Lobachev, A. Y., Vasiliev, S. K., Klementev, A. M., Grebnev, I. E., & Silaev, V. I. (2021). New findings of *Stephanorhinus kirchbergensis* in Siberia. *Palaeontologia Electronica, 24*(1), a14. https://doi.org/10.26879/734

Loose, H. (1975). Pleistocene Rhinocerotidae of W. Europe with reference to the recent two-horned species of Africa and S.E. Asia. *Scripta Geologica, 33*, 1–59.

Madurell-Malapeira, J., Minwer-Barakat, R., Alba, D. M., Garcés, M., Gómez, M., Aurell-Garrido, J., Ros-Montoya, S., Moyà-Solà, S., & Berástegui, X. (2010). The Vallparadís section (Terrassa, Iberian Peninsula) and the latest Villafranchian faunas of Europe. *Quaternary Science Reviews, 29*, 3972–3982. https://doi.org/10.1016/j.quascirev.2010.09.020

Mallet, C., Cornette, R., Billet, G., & Houssaye, A. (2019). Interspecific variation in the limb long bones among modern rhinoceroses—Extent and drivers. *PeerJ, 7*, e7647. https://doi.org/10.7717/peerj.7647

Masini, F., & Sala, B. (2007). Large- and small-mammal distribution patterns and chronostratigraphic boundaries from the Late Pliocene to the Middle Pleistocene of the Italian peninsula. *Quaternary International, 160*, 43–56.

Mazza, P. (1988). The Tuscan Early Pleistocene rhinoceros *Dicerorhinus etruscus*. *Palaeontographica Italica, 75*, 36–87.

Mazza, P., Sala, B., & Fortelius, M. (1993). A small latest Villafranchian (late Early Pleistocene) rhinoceros from Pietrafitta (Perugia, Umbria, Central Italy) with notes on the Pirro and Westerhoven rhinoceroses. *Palaeontographia Italica, 80*, 25–50.

Meier, J. S., Pliatsika, V., & Shelton, K. (2024). The earliest evidence of large animal fossil collecting in mainland Greece at Bronze Age Mycenae. *Science and Reports, 14*, 19158. https://doi.org/10.1038/s41598-024-68778-w

Pandolfi, L. (2011). *Stephanorhinus kirchbergensis* (Jäger, 1839) from the Middle Pleistocene site of Riano (Roma, Central Italy). *Italan Journal of Quaternary Sciences, 24*(1), 103–112.

Pandolfi, L. (2013). Rhinocerotidae (Mammalia, Perissodactyla) from the Middle Pleistoene site of Ponte Milvio, Central Italy. *Bolletino della Societa Paleontologica Italiana, 52*, 219–229. https://doi.org/10.4435/BSPI.2013.25

Pandolfi, L. (2023). Reassessing the phylogeny of Quaternary Eurasian Rhinocerotidae. *Journal of Quaternary Science, 38*(3), 291–294. https://doi.org/10.1002/jqs.3496

Pandolfi, L., Bartolini-Lucenti, S., Cirilli, O., Bukhsianidze, M., Lordkipanidze, D., & Rook, L. (2021a). Paleoecology, biochronology, and paleobiogeography of Eurasian Rhinocerotidae during the Early Pleistocene: The contribution of the fossil material from Dmanisi (Georgia, Southern Caucasus). *Journal of Human Evoluton, 156*, Article 103013. https://doi.org/10.1016/j.jhevol.2021.103013

Pandolfi, L., Cerdeño, E., Codrea, V., & Kotsakis, T. (2017). Biogeography and chronology of the Eurasian extinct rhinoceros *Stephanorhinus etruscus* (Mammalia, Rhinocerotidae). *Comptes Rendus - Palevol, 16*, 762–773.

Pandolfi, L., Codrea, V. A., & Popescu, A. (2019). *Stephanorhinus jeanvireti* (Mammalia, Rhinocerotidae) from the early Pleistocene of Colțești (southwestern Romania). *Comptes Rendus Palevol, 18*(8), 1041–1056. https://doi.org/10.1016/j.crpv.2019.07.004

Pandolfi, L., & Erten, H. (2017). *Stephanorhinus hundsheimensis* (Mammalia, Rhinocerotidae) from the late Early Pleistocene deposits of the Denizli Basin (Anatolia, Turkey). *Geobios, 50*(1), 65–73. https://doi.org/10.1016/j.geobios.2016.10.002

Pandolfi, L., Fiore, I., Gaeta, M., Szabó, P., Vennemann, T., & Tagliacozzo, A. (2018). Rhinocerotidae (Mammalia, Perissodactyla) from the Middle Pleistocene levels of Grotta Romanelli (Lecce, southern Italy). *Geobios, 51*(5), 453–468. https://doi.org/10.1016/j.geobios.2018.08.008

Pandolfi, L., & Petronio, C. (2011). *Stephanorhinus etruscus* (Falconer, 1868) from Pirro Nord (Apricena, Foggia, Southern Italy) with notes on the other late Early Pleistocene Rhinoceros remains of Italy. *Rivista Italiana di Paleontologia e Stratigrafia, 117*(1), 173–187. https://doi.org/10.13130/2039-4942/5969

Pandolfi, L., Pierre-Olivier, A., Bukhsianidze, M., Lordkipanidze, D., & Rook, L. (2021b). Northern Eurasian rhinocerotines (Mammalia, Perissodactyla) by the Pliocene-Pleistocene transition: Phylogeny and historical biogeography. *Journal of Systematic Palaeontology, 19*(15), 1031–1057. https://doi.org/10.1080/14772019.2021.1995907

Pandolfi, L., & Tagliacozzo, A. (2015). *Stephanorhinus hemitoechus* (Mammalia, Rhinocerotidae) from the Late Pleistocene of Valle Radice (Sora, Central Italy) and re-evaluation of the morphometric variability of the species in Europe. *Geobios, 48*(2), 169–191. https://doi.org/10.1016/j.geobios.2015.02.002

Protopopov, A., Potapova, O., Plotnikov, V., Maschenko, E., Boeskorov, G., Klimovskii, A., Banderov, A., Ivanov, S., Kolesov, S., & Pavlov, I. (2015). The frozen mummy of the woolly rhinoceros, *Coelodonta antiquitatis* (Blum., 1799) calf : a new data on early ontogenesis of the extinct species. In *Proceedings of the 75th annual SVP Meeting, Dallas* (p. 199).

Puzachenko, A. Y., Levchenko, V. A., Bertuch, F., Zazovskaya, E. P., & Kirillova, I. V. (2021). Late Pleistocene chronology and environment of woolly rhinoceros (*Coelodonta antiquitatis* (Blumenbach, 1799)) in Beringia. *Quaternary Science Reviews, 263*, Article 106994. https://doi.org/10.1016/j.quascirev.2021.106994

Rivals, F., & Lister, A. (2016). Dietary flexibility and niche partitioning of large herbivores through the Pleistocene of Britain. *Quaternary Science Reviews, 146*, 116–133. https://doi.org/10.1016/j.quascirev.2016.06.007

Sakellariou, E., Koufos, G. D., & Psilovikos, A. (1979). Contribution to the study of Villafranchian in N. Chalkidiki. *Scientific Annals of the Faculty of Physics and Mathematics, Aristoteleian University of Thessaloniki, 19*, 279–296.

Steensma, K. J. (1988). Plio-/Pleistozäne Großsäugetiere (Mammalia) aus dem Becken von Kastoria/Grevena, südlich von Neapolis-NW-Griechenland. Ph.D. Thesis. Clausthal: Technische Universität Clausthal.

Stefanelli, D., Mecozzi, B., Marino, M., Sardella, R., & Breda, M. (2024). The postcranial variability of Quaternary European rhinoceroses: The case study of *Stephanorhinus hundsheimensis* from the Middle Pleistocene site of Contrada Monticelli (Apulia, southern Italy). *Historical Biology*. https://doi.org/10.1080/08912963.2024.2328276

Szabó, P., Kocsis, L., Vennemann, T., Pandolfi, L., Kovács, J., Martinetto, E., & Demény, A. (2017). Pliocene-Early Pleistocene climatic trends in the Italian Peninsula based on stable oxygen and carbon isotope compositions of rhinoceros and gomphothere tooth enamel. *Quaternary Science Reviews, 157*, 52–65. https://doi.org/10.1016/j.quascirev.2016.11.003

Team, R. C. (2020). R: A language and environment for statistical computing. R Foundation for Statistical Computing.

Tong, H. W., & Wang, X. M. (2014). Juvenile skulls and other postcranial bones of *Coelodonta nihowanensis* from Shanshenmiaozui, Nihewan Basin, China. *Journal of Vertebrate Paleontology, 34*(3), 710–724. https://doi.org/10.1080/02724634.2013.814661

Tong, H. W., & Wu, X. Z. (2010). *Stephanorhinus kirchbergensis* (Rhinocerotidae, Mammalia) from the rhino cave in Shennongjia, Hubei. *Chinese Science Bulletin, 55*(12), 1157–1168.

Toula, F. (1902). Das Nashorn von Hundsheim: *Rhinoceros* (*Ceratorhinus* Osborn) *hundsheimensis* nov. form. Mit Ausführungen über die Verhältnisse von elf Schädeln von *Rhinoceros* (*Ceratorhinus*) *sumatrenis*. *Geologische Reichsanstalt, 19*, 1–3.

Tsoukala, E. (2018). Rhinocerotidae from the Late Miocene and Late Pliocene of Macedonia, Greece. A revision of the Neogene—Quaternary Rhinocerotidae of Greece. *Revue de Paleobiologie, 37*, 609–630. https://doi.org/10.5281/zenodo.2545127

Tsoukala, E., & Guérin, C. (2016). The Rhinocerotidae and Suidae of the Middle Pleistocene from Petralona Cave (Macedonia, Greece). *Acta Zoologica Bulgarica, 68*(2), 243–264.

Uzunidis, A., Antoine, P. O., & Brugal, J. P. (2022). A Middle Pleistocene *Coelodonta antiquitatis praecursor* Guérin (1980) (Mammalia, Perissodactyla) from Les Rameaux, SW France, and a revised phylogeny of *Coelodonta* Bronn, 1831. *Quaternary Science Reviews, 288*, Article 107594. https://doi.org/10.1016/j.quascirev.2022.107594

Vislobokova, I. A., & Agadjanian, A. K. (2015). New data on large mammals of the Pleistocene Trlica fauna Montenegro, the Central Balkans. *Paleontological Journal, 49*(6), 651–667. https://doi.org/10.1134/S0031030115060143